

Feature engineering and symbolic regression methods for detecting hidden physics from sparse sensors

Harsha Vaddireddy,¹ Adil Rasheed,² Anne E Staples,³ and Omer San^{1, a)}

¹⁾*School of Mechanical & Aerospace Engineering, Oklahoma State University, Stillwater, OK 74078, USA.*

²⁾*Department of Engineering Cybernetics, Norwegian University of Science and Technology, N-7465, Trondheim, Norway.*

³⁾*Department of Biomedical Engineering and Mechanics, Virginia Tech, Blacksburg, VA 24061, USA.*

(Dated: 29 June 2022)

In this study we put forth a modular approach for distilling hidden flow physics in discrete and sparse observations. To address functional expressibility, a key limitation of the black-box machine learning methods, we have exploited the use of symbolic regression as a principle for identifying relations and operators that are related to the underlying processes. This approach combines evolutionary computation with feature engineering to provide a tool to discover hidden parameterizations embedded in the trajectory of fluid flows in the Eulerian frame of reference. Our approach in this study mainly involves gene expression programming (GEP) and sequential threshold ridge regression (STRidge) algorithms. We demonstrate our results in three different applications: (i) equation discovery, (ii) truncation error analysis, and (iii) hidden physics discovery, for which we include both predicting unknown source terms from a set of sparse observations and discovering subgrid scale closure models. We illustrate that both GEP and STRidge algorithms are able to distill the Smagorinsky model from an array of tailored features in solving the Kraichnan turbulence problem. Our results demonstrate the huge potential of these techniques in complex physics problems, and reveal the importance of feature selection and feature engineering in model discovery approaches.

Keywords: Symbolic regression, gene expression programming, compressive sensing, model discovery, modified equation analysis, hidden physics discovery

I. INTRODUCTION

Since the dawn of mathematical modelling of complex physical process, scientists have been attempting to formulate predictive models to infer current and future states. These first principle models are generally conceptualized from conservation laws, sound physical arguments and empirical heuristics drawn from either conducting experiments or hypothesis made by an insightful researcher. However, there are many complex systems (some being climate science, weather forecasting and disease control modeling) with their governing equations known partially and their hidden physics await to be modelled. In last decade, there has been rapid advances in machine learning^{1,2} and easy access to rich data, thanks to plummeting costs of sensors and high performance computers.

This paradigm shift in data driven techniques can be readily exploited to distill new or improved physical models for nonlinear dynamical systems. Extracting predictive models based on observing complex patterns from vast multimodal data can be loosely termed as reverse engineering nature. This approach is not particularly new, for example Kepler used planets' positional data to approximate the elliptic orbits. The reverse engineering approach is most appropriate in modern age as we can leverage computers to directly infer physical laws from data collected from omnipresent sensors that otherwise might not be

^{a)}Electronic mail: osan@okstate.edu

comprehensible to humans. Symbolic regression methods are a class of data driven algorithms that aims to find a mathematical model that can describe and predict hidden physics from observed input-response data. Some of the popular machine learning techniques that are adapted for the task of symbolic regression are neural networks^{3,4}, compressive sensing/sparse optimization^{5,6}, and evolutionary algorithms^{7,8}.

Symbolic regression (SR) approaches based on evolutionary computation^{7,9} are class of frameworks that are capable of finding analytically tractable function. Traditional deterministic regression algorithms assume a mathematical form and only find parameters that best fit the data. On the other hand, evolutionary SR approaches aim to simultaneously find parameters and also learn functional form of the model from input-response data. Evolutionary algorithms search for functional abstractions with preselected set of mathematical operators and operands, while minimizing the error metrics. Furthermore, the optimal model is selected from Pareto front analysis with respect to minimizing accuracy versus model complexity. Genetic programming (GP)⁷ is popular choice leveraged by most of the SR frameworks. GP is an extended and improved version of genetic algorithm (GA)^{10,11} which is inspired from Darwin's theory of natural evolution. A seminal work was done in identifying hidden physical laws^{12,13} from input-output response using GP approach. GP has been applied in the context of SR approach in digital signal processing¹⁴, nonlinear system identification¹⁵ and aerodynamic parametric estimation¹⁶. Furthermore, GP as SR tool was applied to identify complex closed-loop feedback control laws for turbulent separated flows¹⁷⁻¹⁹. Hidden physical laws of evolution of harmonic oscillator based on sensor measurements and real world prediction of solar powered production of a site based on energy production values and weather forecast was identified using GP as SR approach²⁰.

Improved versions of GP focus on better representation of chromosome, that helps in free evolution of chromosome with constraint on complexity of its growth and faster search for best chromosome. Some of these improved versions of GP are gene expression programming (GEP)⁸, parse matrix evolution (PME)²¹ and linear genetic programming (LGP)²². GEP takes advantage of linear coded chromosome approach from GA and parse tree evolution of GP to alleviate the disadvantages of both GA and GP. GEP was applied to diverse application as SR tool to recover nonlinear dynamical systems²³⁻²⁶. Recently, GEP was modified for tensor regression termed as multi-GEP and has been applied to recover functional models approximating nonlinear behavior of stress tensor in Reynolds-averaged Navier-Stokes (RANS)²⁷. Furthermore, this novel algorithm was extended to identify closure models in combustion setting for large eddy simulations (LES)²⁸ and fitting new SR discovered damping function in hybrid RANS/LES methodology²⁹. Generally, evolutionary based SR approaches can identify models with complex nonlinear compositions given enough computational time.

Compressive sensing (CS)^{5,6} is predominately applied to signal processing in seeking the sparsest solution (i.e., solution with the fewest number of features). Basis pursuit algorithms³⁰ also identified as sparsity promoting optimization techniques^{31,32} play fundamental role in CS. Ordinary least square (OLS) optimization generally results in identifying models with large complexity which are prone to overfitting. In sparse optimization, the OLS objective function is regularized by adding additional constraint on coefficient vector. This regularization helps in taming and shrinking large coefficients and thereby promoting sparsity in feature selection and avoiding overfitted solutions. The least absolute shrinkage and selection operator (LASSO)^{31,33} is one of the most popular regularized LS regression methods. In LASSO L_1 penalty is added to LS objective function to recover sparse solutions³⁴. In Bayesian terms, LASSO is maximum a posteriori estimate (MAP) of LS with Laplacian prior. LASSO performs feature selection and simultaneously shrinks large coefficients which may manifest to overfit the training data. Ridge regression³⁵ is another regularized variant where L_2 penalty is added to LS objective function. Ridge regression is also defined as MAP estimate of LS with Gaussian prior. The L_2 penalty helps in grouping multiple correlated basis functions and increases robustness and convergence stability for ill conditioned systems. Elastic net approach^{36,37} is a hybrid of LASSO and ridge approach combining the strengths of both algorithms.

Derived from these advances, seminal work was done in employing sparse regression to identify physical laws of nonlinear dynamical systems³⁸. This work leverages the structure of sparse physical laws i.e., only few terms represent the dynamics. They construct a large feature library of potential basis functions that has the expressive power to define the dynamics and then seek to find sparse feature set from this overdetermined system. To achieve this, they introduce sequentially threshold least squares (STLS) algorithm³⁸, where a hard threshold on OLS coefficient estimates was performed recursively to retain only small number of coefficients thereby finding sparse solutions. This algorithm was leveraged to form a framework called sparse identification of nonlinear dynamics (SINDy)³⁸ to extract physical laws of nonlinear dynamical systems represented by ordinary differential equations (ODE). This novel work re-envisioned the model discovery from the perspective of sparse optimization and compressive sensing. SINDy framework recovered various benchmark dynamical systems such as chaotic Lorenz system and vortex shedding behind the cylinder. However, STLS regression finds it challenging to discover physical laws that are represented by spatio-temporal data or high-dimensional measurements and has highly correlated features in the basis library. This limitation was addressed using regularized variant of STLS called sequentially threshold ridge regression (STRidge) algorithm³⁹. This algorithm was intended to discover unknown governing equations that are represented by partial differential equations (PDEs) hence forming a framework termed as PDE-functional identification of nonlinear dynamics (PDE-FIND)³⁹. PDE-FIND was applied to recover canonical PDEs representing various nonlinear dynamics. This framework also performs reasonably well under addition of noise to data/measurements. These sparse optimization frameworks generally have a free parameter associated with regularization term that is tuned by the user to recover models with high complexity to models that are parsimonious.

In the similar direction of discovering governing equations using sparse regression techniques, L_1 regularized LS minimization was used to recover various nonlinear PDEs^{40,41} using both high fidelity and distorted (noise) data. Additionally, limited and distorted data samples were used to recover chaotic and high-dimensional nonlinear dynamical systems^{42,43}. To automatically filter models with respect to model complexity (number of terms in the model) versus test accuracy, Bayes information criteria was used to rank most informative models⁴⁴. Furthermore, SINDy coupled with model information criteria is used to infer canonical biological models⁴⁵ and introduce general reduced order modelling framework⁴⁶. STRidge³⁹ was applied as a deterministic symbolic regression method to derive algebraic Reynolds-stress models for the RANS equations⁴⁷. Recently, various sparse regression algorithms like LASSO³¹, STRidge³⁹, sparse relaxed regularized regression⁴⁸ and forward backward greedy algorithm⁴⁹ were investigated to recover truncation error terms of various modified differential equations (MDEs) coming from canonical PDEs⁵⁰. The above discussed frameworks assume that the structure of the model to be recovered is sparse in nature; that is only a small number of terms govern the dynamics of the system. This assumption holds for many physical systems in science and engineering.

Fast function extraction (FFX)⁵¹ is another deterministic symbolic regression approach based on pathwise regularized learning that is also called elastic net algorithm³⁶. The resulting models of FFX are selected through non-dominated filtering with respect to accuracy and model complexity similar to evolutionary computations. FFX is influenced from both GP and CS to better distill physical models from data. FFX has been applied to recover hidden physical laws²⁰, canonical governing equations⁵² and Reynolds stress models for RANS equations⁵³. Some other potential algorithms for deterministic SR are elite base regression (EBR)⁵⁴ and prioritized grammar enumeration (PGE)⁵⁵. EBR uses only elite features in search space selected by measuring correlation coefficient of features with respect to the target model. PGE is another deterministic approach that aims for the substantial reduction of search space where genetic operators and random numbers from GP are replaced with grammar production rules and systematic choices.

Artificial neural network (ANN) also referred to as deep learning (if multiple hidden layers are used) is a machine learning technique that transforms input features through nonlinear interactions and maps to output target feature^{3,4}. ANNs attracted attention in

recent times due to their exemplary performance in modeling complex nonlinear interactions across a wide range of applications including image processing⁵⁶, video classification⁵⁷ and autonomous driving⁵⁸. ANNs produce black box models that are quite not open to physical inference or interpretability. Recently, physics informed neural networks (PINNs)⁵⁹ were proposed in flavour of SR that are capable of identifying scalar parameters for known physical models. PINNs used loss function in symbolic form to help ANNs constraint to physical structure of the system. In the similar lines, Gaussian process was also investigated for discovery of coefficients by recasting unknown coefficients as GP kernel hyper-parameters for various time dependent PDEs⁶⁰. Convolutional neural networks (CNNs) are constructed to produce hidden physical laws from using the insight of establishing direct connections between filters and finite difference approximations of differential operators^{61,62}. This novel approach has been demonstrated to discover underlying PDEs from learning the filters by minimizing the loss functions^{63,64}.

In this paper, we demonstrate the use of evolutionary computation algorithm, GEP and sparse regression algorithm, STRidge in the context of SR approach to discover various physical laws represented by linear and nonlinear PDEs from observing input-response data. We begin by demonstrating identification of canonical linear and nonlinear PDEs that are upto fifth order in space. For identifying one particular PDE, we demonstrate natural feature extraction ability of GEP and the limit of expressive and prediction power of feature library when dealing with STRidge in discovering physical laws. We then demonstrate the discovery of highly nonlinear truncation error terms of Burgers MDE using both GEP and STRidge. Following truncation error terms identification, we apply GEP using sparse data to recover hidden source term represented by complex function composition of 1D advection-diffusion process and 2D vortex-merger problem. Furthermore, both GEP and STRidge are used to demonstrate the identification of eddy viscosity kernel along with its ad-hoc modelling coefficient closing LES equations simulating 2D decaying turbulence problem.

The rest of the paper is organized as follows. Section II gives a brief description of the GEP and STRidge algorithm. In Section III, GEP and STRidge are tested on identifying different canonical PDEs. Section IV deals with identification of nonlinear truncation terms of Burgers MDE using both STRidge and GEP. In Section V we exploit GEP for identification of hidden source term of 1D advection-diffusion process and 2D vortex-merger problem. We additionally demonstrate the recovery of eddy viscosity kernel and its modelling coefficient by both GEP and STRidge for closing LES equations simulating 2D decaying turbulence problem in same section. Finally, Section VI draws our conclusions and highlights some ideas for future extension of this work.

II. METHODOLOGY

We recover various physical models from data using two symbolic regression tools namely, GEP an evolutionary computing algorithm and STRidge which is a deterministic algorithm that draws its influences from compressive sensing and sparse optimization. We take the example of equation discovery problem that is discussed in Section III to elaborate the methodology of applying GEP and STRidge for recovering various physical models. In Section III, above mentioned SR tools are exploited to identify linear and nonlinear spatial derivative terms resulting in identification of various canonical PDEs from observing spatio-temporal data. In the current paper, we restrict the PDEs to be recovered to quadratic nonlinear and up to fifth order in space. The general nonlinear PDE to be recovered is in the form of,

$$u_t = \mathcal{F}(\sigma, u, u^2, u_x, u_x^2, uu_x, u_{2x}, \dots, u_{5x}^2), \quad (1)$$

where subscripts denote order of partial differentiation and σ is an arbitrary parameter. For example, consider the problem of identifying viscous Burgers equation as shown below,

$$u_t + uu_x = \nu u_{2x}, \quad (2)$$

where $u(x, t)$ is generally velocity field and ν is viscous coefficient. The solution field $u(x, t) \in \mathbb{R}^{m \times n}$ where m is the number of time snapshots and n is number of spatial locations. The solution field $u(x, t)$ is generally obtained by solving Eq. 2 analytically or numerically and in real world using sensors measurements. The solution field $u(x, t)$ is arranged as shown below,

$$\mathbf{u} = \left[\begin{array}{cccc} u_1(t_1) & u_2(t_1) & \dots & u_n(t_1) \\ u_1(t_2) & u_2(t_2) & \dots & u_n(t_2) \\ \vdots & \vdots & \ddots & \vdots \\ u_1(t_m) & u_2(t_m) & \dots & u_n(t_m) \end{array} \right] \left. \right\} \text{time snapshots} \quad (3)$$

For recovering PDEs, we need to construct library of basis functions called as feature library that contains higher order derivatives of solution field $u(x, t)$. Higher order spatial and temporal partial derivative terms can be approximated using any available numerical schemes once the recording of discrete data set given by Eq. 3 is available. In our current setup, we use the leapfrog scheme for approximating the temporal derivatives and central difference schemes for space derivatives as follows,

$$\left. \begin{array}{l} u_t = \frac{u_j^{p+1} - u_j^{p-1}}{2dt} \\ u_{2t} = \frac{u_j^{p+1} - 2u_j^p + u_j^{p-1}}{dt^2} \\ u_x = \frac{u_{j+1}^p - u_{j-1}^p}{2dx} \\ u_{2x} = \frac{u_{j+1}^p - 2u_j^p + u_{j-1}^p}{dx^2} \\ u_{3x} = \frac{u_{j+2}^p - 2u_{j+1}^p + 2u_{j-1}^p - u_{j-2}^p}{2dx^3} \\ u_{4x} = \frac{u_{j+2}^p - 4u_{j+1}^p + 6u_j^p + 4u_{j-1}^p - u_{j-2}^p}{dx^4} \\ u_{5x} = \frac{u_{j+3}^p - 4u_{j+2}^p + 5u_{j+1}^p - 5u_{j-1}^p + 4u_{j-2}^p - u_{j-3}^p}{2dx^5} \end{array} \right\} \quad (4)$$

where temporal and spatial step is given by dt and dx respectively. In Eq. 4, the spatial location is denoted using subscript index j and the time using superscript index p .

We note that other difference schemes such as automatic differentiation or spectral differentiation for periodic domain can be easily used within our study. Both GEP and STRidge take the input library consisting of features (basis functions) that are built using Eq. 2 and Eq. 3. This core library used for equation discovery in Section III is shown below,

$$\left. \begin{array}{l} \mathbf{V}(t) = [\mathbf{U}_t] \\ \tilde{\Theta}(\mathbf{U}) = [\mathbf{U} \ \mathbf{U}_x \ \mathbf{U}_{2x} \ \mathbf{U}_{3x} \ \mathbf{U}_{4x} \ \mathbf{U}_{5x}] \end{array} \right\} \quad (5)$$

Each column in Eq. 5, the solution $u(x, t)$ and its derivatives in space and time are arranged with size $m \cdot n \times 1$ where m is the number of time snapshots and n is the spatial locations. For example, the features (basis functions) \mathbf{U} and \mathbf{U}_{2x} are arranged as follows:

$$\mathbf{U} = \left[\begin{array}{c} u(x_0, t_0) \\ u(x_0, t_1) \\ \vdots \\ u(x_j, t_p) \\ \vdots \\ u(x_n, t_m) \end{array} \right], \quad \mathbf{U}_{2x} = \left[\begin{array}{c} u_{2x}(x_0, t_0) \\ u_{2x}(x_0, t_1) \\ \vdots \\ u_{2x}(x_j, t_p) \\ \vdots \\ u_{2x}(x_n, t_m) \end{array} \right], \quad (6)$$

where subscript j denotes the spatial location and subscript p denotes the time snapshot. The features (basis functions) in core library $\tilde{\Theta}(\mathbf{U})$ is expanded to include interacting features limiting to quadratic nonlinearity and also a constant term. The final expanded library is in the form,

$$\Theta(\mathbf{U}) = [\mathbf{1} \ \mathbf{U} \ \mathbf{U}^2 \ \mathbf{U}_x \ \mathbf{U}\mathbf{U}_x \ \mathbf{U}_x^2 \ \dots \ \mathbf{U}_{5x}^2] \quad (7)$$

where the size of library is $\Theta(\mathbf{U}) \in \mathbb{R}^{m \cdot n \times N_\beta}$ and N_β is number of features (basis functions) (i.e., $N_\beta = 28$). For example, if we have 501 spatial points and 101 time snapshots with 28 bases then $\Theta(\mathbf{U})$ (Eq. 7) contains 501×101 rows and 28 columns.

Note that the core feature library $\tilde{\Theta}(\mathbf{U})$ in Eq. 5 is given as input to GEP to recover PDEs and the algorithm extracts higher degree nonlinear interactions of core features in $\tilde{\Theta}(\mathbf{U})$. However, for sparse optimization techniques such as STRidge, explicit input of all possible combinations of core features in Eq. 5 are required. Therefore, $\Theta(\mathbf{U})$ in Eq. 7 forms the input to STRidge algorithm for equation identification. This forms the fundamental difference in terms of feature building for both algorithms. The following Subsection II A describe brief introduction to GEP and its specific hyper-parameters that control the algorithms efficacy of identifying the physical models from observing data. Furthermore the Subsection II B describes how to form linear system representation in terms of $\mathbf{V}(\mathbf{t})$ and $\Theta(\mathbf{U})$ and briefly describe STRidge optimization approach to identify sparse features and thereby building parsimonious models using spatio-temporal data.

A. Gene Expression Programming

Gene expression programming (GEP)^{8,65} is a genotype-phenotype evolutionary optimization algorithm which takes advantage of simple chromosome representative of genetic algorithm (GA)¹⁰ and free expansion of complex chromosomes of genetic programming (GP)⁷. As in most evolutionary algorithms, this technique also starts with generating initial random populations, iteratively selecting candidate solution according to a fitness function and improving candidate solutions by modifying through genetic variations using one or more genetic operators. The main difference between GP and GEP is how both techniques define the nature of their individuals. In GP, the individuals are nonlinear entities of different sizes and shapes represented as parse trees and in GEP the individuals are encoded as linear strings of fixed length called genome or chromosome similar to GA representation and later expressed as nonlinear entities of different sizes and shapes called phenotype or expression trees (ET). GEP is introduced for very broad range of applications, but here it is introduced as symbolic regression tool to extract constraint free solutions from observing input-response data.

The arrangement of typical gene/chromosome in GEP is shown in Fig. 1. The GEP gene is typically composed of head and tail region shown in colored box in Fig. 1. The head of a gene consists of both symbolic terms from functions (elements from function set F) and terminals (elements from terminal set T) where as the tail consists of only terminals. The function set F may contain arithmetic mathematical operators (e.g., $+$, \times , $-$, $/$), nonlinear functions (e.g., \sin , \cos , \tan , \arctan , $\sqrt{}$, \exp) or Boolean operators (e.g., Not , Nor , Or , And) and terminal set contains the symbolic variables that our function may depend on. The gene always starts with a randomly generated mathematical operator from function set F . The head length is one of the important hyper-parameters of GEP which is determined using trial and error method as there is no definite method to assign it. Once head length is determined, the size of tail is determined as a function of head length and maximum arity of a mathematical operator takes in the function set (F)⁹. It can be calculated by following equation,

$$\text{tail length} = \text{head length} \times (a_{\max} - 1) + 1, \quad (8)$$

where a_{\max} is maximum argument of a function in F . The single gene can be extended to multigenic chromosomes where individual genes are linked using linking function (eg.,

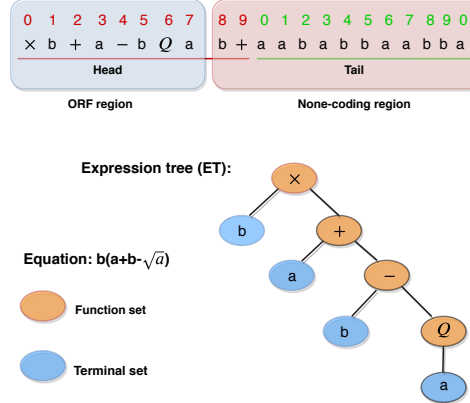


FIG. 1. ET of a gene/chromosome with its structure in GEP. Q represent square root operator.

$+, \times, /, -$). General rule of thumb is to have larger head and more number of genes when dealing with complex problems⁹.

The structural organization of GEP gene is arranged in terms of open reading frames (ORFs) inspired from biology where coding sequence of a gene equivalent to ORFs begins with start codon, continue with amino acid codon and ends with termination codon. Contrast to gene in biology, in GEP the start site is always the first position of a gene, but the termination point does not always coincide with last position of a gene. These regions of gene are termed as non coding regions downstream of the termination point. Only the ORF region is expressed as ET and can be clearly seen in Fig. 1.

Even though the none-coding regions in GEP genes are not participated in final solution, the power of GEP evolvability lies in this region. The syntactically correct genes in GEP evolve after modification through diverse genetic operators due to this region chromosome. This is the paramount difference between GEP and GP implementations where in latter, many syntactically invalid individuals are produced and need to be discarded while evolving the solutions and additional special constraint on the depth/complexity of candidate solution to be evolved to avoid bloating problem¹⁹.

Fig. 2 shows the typical flowchart of GEP algorithm. The process is described briefly below,

1. The optimization procedure starts with a random generation of chromosomes built upon combinations of functions and terminals. The number of random population to initialize is a hyper-parameter and larger the population size, better the probability of finding best candidate solution.
2. After the population generation, the chromosomes are expressed as ETs and also as mathematical model which is to be evaluated using a fitness function. In our setup, we use mean squared error between best predicted model f^* and true model f as fitness function.

$$MSE = \frac{1}{N} \sum_{l=1}^N \left(f_{(lk)}^* - f_{(l)} \right)^2, \quad (9)$$

where f_{lk}^* is the value predicted by the chromosome k for fitness case l (out of N samples cases) and f_l is the true or measurement value for l fitness case.

3. The termination criteria is checked after all fitness evaluations, to continue evolving or to save the best fitness chromosome as our final predicted model. In our current setup, we terminate after specified number of generations.

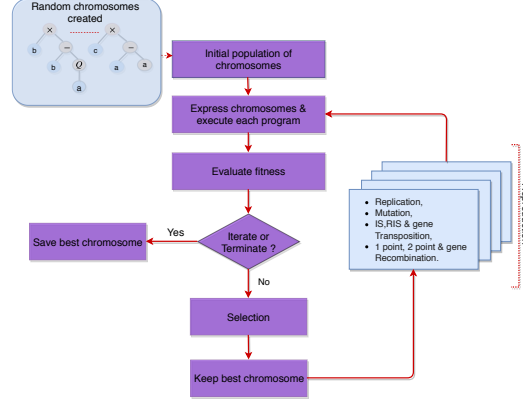


FIG. 2. Flowchart of gene expression programming.

4. The evolvability/reproduction of chromosome through genetic operators which is core part of GEP evolutionary algorithm executes if termination criteria is not met. Before the genetic operations on chromosome begins, the best chromosome according to fitness function is cloned to next generations using a selection method. Popular selection methods include tournament selection with elitism and roulette-wheel selection with elitism. In our current setup we use tournament selection with elitism.
5. The four genetic operators that introduce variation in populations are mutation, inversion, transposition and recombination. The GEP transposition operator is applied to the elements of chromosome in three ways: insertion sequence (IS), root insertion sequence (RIS) and gene insertion sequence and similarly three kinds of recombination are applied namely one point, two point and gene recombination.
6. The process is continued up to termination criteria is met, that is number of generations in our current setup.

TABLE I. GEP hyper-parameters for various genetic operators selected for all the test cases in this study.

Hyper-parameters	Value
Selection	Tournament selection
Mutation rate	0.05
Inversion	0.1
IS transposition rate	0.1
RIS transposition rate	0.1
Gene transposition rate	0.1
One point recombination	0.3
Two point recombination	0.2
Gene recombination	0.1
Dc specific mutation rate	0.05
Dc specific inversion rate	0.1
Dc specific transposition rate	0.1
Random constant mutation rate	0.02

Numerical constants occur in most mathematical models and, therefore, it is important to any symbolic regression tools to effectively integrate floating point constants in their optimization search. GP⁷ handles numerical constants by introducing random numerical constants in a specified range to its parse trees. The random constants are moved around the parse trees using crossover operator. GEP handles creation of random numerical constants (RNCs) by using a extra terminal ‘?’ and a separate domain Dc composed of symbols chosen to represent random numerical constants⁹. This Dc specific domain starts from the end of a tail of the gene.

For each gene, RNCs are generated during the creation of random initial population and kept in array. To maintain the genetic variations in the pool of RNCs, additional genetic operators are introduced to take effect on Dc specific regions. Hence in addition to the usual genetic operators such as mutation, inversion, transposition and recombination, GEP-RNC algorithm has Dc specific inversion, transposition and random constant mutation operators. Hence with these modifications to algorithm appropriate diversity of random constants can be generated and evolved through operations of genetic operators. The values for each genetic operator selected for this study are listed in Table I. These values are selected from various examples given in⁹ combined with trial and error approach. Additionally, to simplify our study, we kept these parameters same for all the test cases even though they may not be the best values for the test case under investigation.

Once decent values of genetic operators that can explore the search space are selected, the size of head length, population and number of genes forms the most important hyper-parameters of GEP. Generally, larger head length and more number of genes are selected for identifying complex expressions. More number of population helps in diverse set of initial candidates which may help GEP in finding the best chromosome in less number of generations. However, computational overhead increases with increase in the size of population. Furthermore, best chromosome can be identified in less generations with right selection of linking function between genes. GEP algorithm inherently performs poor in predicting numerical constants that are ubiquitous in any physical laws. Hence, GEP-RNC algorithm is used where a range of random constants are predefined to help GEP to find numerical constants. This also forms important in GEP identifying the underlying expression in less number of generations. Finally, we note that due to heuristic nature of evolutionary algorithms, any other combinations of hyper-parameters might work perfectly in identifying the symbolic expressions. In this study, we used geppy⁶⁶, a open source library for symbolic regression using GEP which is built as an extension to distributed evolutionary algorithms in python (DEAP) package⁶⁷.

B. Sequential Threshold Ridge Regression

Compressive sensing/sparse optimization^{5,68} have been exploited for sparse feature selection from a large library of potential candidate features and recovering dynamical systems represented by ODEs and PDEs^{38,39,44} in a highly efficient computational manner. In our setup, we use this STRidge³⁹ algorithm to recover various hidden physical models from observing data. In continuation with the Section II where we define feature library $\Theta(\mathbf{U})$ and target/output data $\mathbf{V}(t)$, this subsection briefly explains the formation of overdetermined linear system for STRidge optimization to identify various physical models from data.

The Burgers PDE given in Eq. 2 or any other PDE under consideration can be written in the form of linear system representation in terms of $\Theta(\mathbf{U})$ and $\mathbf{V}(t)$,

$$\mathbf{V}(t) = \Theta(\mathbf{U}) \cdot \boldsymbol{\beta} \quad (10)$$

where $\boldsymbol{\beta} = [\beta_1, \beta_2, \dots, \beta_{N_\beta}]$ is coefficient vector of size \mathbb{R}^{N_β} where N_β is number of features (basis functions) in library $\Theta(\mathbf{U})$. Note that the $\Theta(\mathbf{U})$ is an over-complete library (number of measurements greater than features) and having rich feature (column) space to represent the dynamics under consideration. Thus we form a linear system problem in Eq. 10 with

over-determined system. The goal of STRidge is to find sparse coefficient vector β that only consists of active features that best represent dynamics and rest of features set to zero. For example, in Burgers equation given by Eq. 2, STRidge ideally has to find coefficient vector β that corresponds with the features uu_x and u_{2x} and simultaneously set all others features to zero.

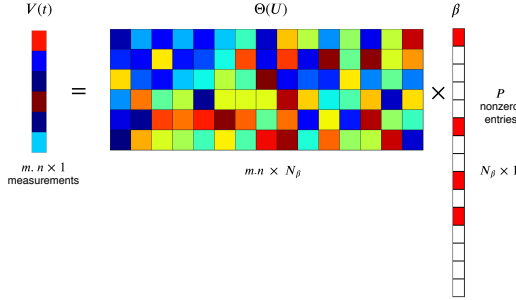


FIG. 3. Structure of compressive matrices with sparse non zero entries in coefficient vector β . Red boxes in β vector correspond to active features coefficients and all other coefficients being set to zero.

The linear system defined in Eq. 10 can be solved for β using the ordinary least squares (OLS) problem. But OLS minimization tries to form functional relationship with all the features in $\Theta(U)$ resulting in all non zero values in coefficient vector β . Thus solving Eq. 10 using OLS infers radically complex functional form to represent the underlying PDE and generally results in overfitted models. Regularized least square minimization can be applied to constraint the coefficients and avoid overfitting. Hence regularized LS optimization is preferred to identify the sparse features (basis functions) along with their coefficient estimation. Typical estimation of sparse coefficient vector with P non zero entries in β is shown in Fig. 3. General sparse regression objective function to approximate the solution of coefficient vector β is given by,

$$\beta^* = \arg \min_{\beta} \|\Theta \cdot \beta - \mathbf{V}(\mathbf{t})\|_2^2 + \lambda \|\beta\|_0 \quad (11)$$

where λ is regularizing weight and $\|\beta\|_0$ corresponds to L_0 penalty which makes the problem np -hard. Hence to arrive at convex optimization problem of Eq. 12, L_1 and L_2 penalty are generally used to approximate the solution of coefficient vector β .

The addition of L_1 penalty to LS objective function which corresponds to maximum a posteriori estimate (MAP) of Laplacian prior and termed as least absolute shrinkage and selection operator (LASSO) in compressive sensing. It is defined by,

$$\beta^* = \arg \min_{\beta} \|\Theta \cdot \beta - \mathbf{V}(\mathbf{t})\|_2^2 + \lambda \|\beta\|_1 \quad (12)$$

However, LASSO tends to suffer from feature selection when feature space is correlated³⁹. Sequential threshold least squares (STLS) was proposed to identify dynamical systems represented by ODEs³⁸. In STLS, hard threshold is performed on least square estimates of regression coefficients and recursively performing the hard thresholding on remaining non zero coefficients. However, STLS also finds challenging in identification of systems with multiple correlated columns in Θ . Hence L_2 regularized least squares termed as ridge regression³⁵ which corresponds to maximum a posteriori estimate using a Gaussian prior is proposed to handle identification of PDEs. Ridge regression is defined by,

$$\begin{aligned} \beta^* &= \arg \min_{\beta} \|\Theta \cdot \beta - \mathbf{V}(\mathbf{t})\|_2^2 + \lambda \|\beta\|_2 \\ &= (\Theta^T \Theta + \lambda^2 I) \Theta^T \mathbf{V}(\mathbf{t}) \end{aligned} \quad (13)$$

Ridge regression is substituted for ordinary least squares in STLS and termed the resulting algorithm as sequential threshold ridge regression (STRidge)³⁹. The STRidge framework³⁹ is illustrated in Algorithm 1 for the sake of completeness. Note that, if $\lambda = 0$, the STRidge become STLS procedure. For more elaborate details on updating tolerance (tol) to perform hard thresholding in Algorithm 1 readers are encouraged to refer supplementary document of Rudy et al³⁹.

Algorithm 1: STRidge(Θ , $\mathbf{V}(\mathbf{t})$, λ , tol , iters)³⁹

Input: Θ , $\mathbf{V}(\mathbf{t})$, λ , tol , iters
Output: β^*
 $\beta^* = \arg \min_{\beta} \|\Theta \cdot \beta - \mathbf{V}(\mathbf{t})\|_2^2 + \lambda \|\beta\|_2^2$
 $large = \{p : |\beta_p^*| \geq tol\}$
 $\beta^*[large] = 0$
 $\beta^*[large] = \text{STRidge}(\Theta[:, large], \mathbf{V}(\mathbf{t}), \lambda, tol, \text{iters} - 1)$
return β^*

We use the framework provided by Rudy et al.,³⁹ in our current study. The hyper-parameters in STRidge include regularization weight λ and tolerance level tol which are to be tuned to identify appropriate physical models. In the current study, the sensitivity of feature coefficients for various values of λ 's and final value of λ where the best model is identified is showed. The following sections deal with various numerical experiments to test GEP and STRidge frameworks.

III. EQUATION DISCOVERY

Partial differential equations (PDEs) play a prominent role in all branches of science and engineering. They are generally derived from conservation laws, sound physical arguments and empirical heuristic from an insightful researcher. Recent explosion of machine learning algorithms provides new ways to identify hidden physical laws represented by PDEs using only data. In this section we demonstrate the identification of various linear and nonlinear canonical PDEs using GEP and STRidge algorithms from using only data. Analytical solutions of PDEs are used to collect the data. Table II summarizes various PDEs along with their analytical solutions $u(t, x)$ and domain discretization. Building feature library and corresponding response data to identify PDEs is discussed in detail in Section II.

We reiterate the methodology for PDE identification in Section II. The analytical solution $u(t, x)$ is solved at discrete spatial and temporal locations resulting from discretization of space and time domain as given in Table II. The discrete analytical solution is used as input data for calculating higher order spatial and temporal data using finite difference approximations listed in Eq. 4. Furthermore, feature library is built using discrete solution $u(t, x)$ and higher order derivative which is discussed in Section II. As GEP is a natural feature extractor, core feature library $\tilde{\Theta}(\mathbf{U})$ given in Eq. 5 is enough to form input data i.e., GEP terminal set. Table V shows the function set and terminal set used for equation identification and Table I lists the hyper-parameter values for various genetic operators. However, extended core feature library $\Theta(\mathbf{U})$ which contains the higher degree interactions of features is used as input for STRidge as expressive power of STRidge depends on exhaustive combinations of features in the input library. The temporal derivative of $u(t, x)$ is target or response data $\mathbf{V}(\mathbf{t})$ given in Eq. 5 for both GEP and STRidge.

A. Wave Equation

Our first test case is wave equation which is a first order linear PDE. The PDE and its analytical solution is listed in Table II. We choose constant wave speed $a = 1.0$ for propagation of solution $u(t, x)$. Fig. 4 shows the analytical solution $u(t, x)$ of wave equation.

TABLE II. Summary of canonical PDEs selected for recovery.

PDE	Exact solution	Physical parameters	Discretization
			n (spatial) m (temporal)
Wave eq. $u_t = -au_x$	$u(t, x) = \sin(2\pi(x - at))$	$a = 1.0$	$x \in [0, 1]$ ($n = 101$), $t \in [0, 1]$ ($m = 101$)
Heat eq. $u_t = -\alpha u_{2x}$	$u(t, x) = -\sin(x)\exp(-t)$	$\alpha = 1.0$	$x \in [-\pi, \pi]$ ($n = 201$), $t \in [0, 1]$ ($m = 101$)
Burgers eq. (i) $u_t = -uu_x + \nu u_{2x}$	$u(t, x) = \frac{x}{(t+1) \left((1 + \sqrt{(t+1)})\exp(-\frac{1}{16\nu} \frac{4x^2 - t - 1}{(t+1)}) \right)}$	$\nu = 0.01$	$x \in [0, 1]$ ($n = 101$), $t \in [0, 1]$ ($m = 101$)
Burgers eq. (ii) $u_t = -uu_x + \nu u_{2x}$	$u(t, x) = \frac{2\nu\pi\exp(-\pi^2\nu t)\sin(\pi x)}{a + \exp(-\pi^2\nu t)\cos(\pi x)}$	$\nu = 0.01$, $a = 5/4$	$x \in [0, 1]$ ($n = 101$), $t \in [0, 100]$ ($m = 101$)
Korteweg-de Vries eq. $u_t = -\alpha uu_x - \beta u_{3x}$	$u(t, x) = 12 \left(\frac{4\cosh(2x - 8t) + \cosh(4x - 64t) + 3}{(3\cosh(x - 28t) + \cosh(3x - 36t))^2} \right)$	$\alpha = 6.0$, $\beta = 1.0$	$x \in [-10, 10]$ ($n = 501$), $t \in [0, 1]$ ($m = 201$)
Kawahara eq. $u_t = -uu_x - \alpha u_{3x} - \beta u_{5x}$	$u(t, x) = \frac{105}{169} \operatorname{sech} \left(\frac{1}{2\sqrt{13}} (x - at) \right)^4$	$\alpha = 1.0$, $\beta = 1.0$, $a = 36/169$	$x \in [-20, 20]$ ($n = 401$), $t \in [0, 1]$ ($m = 101$)
Newell-Whitehead-Segel eq. $u_t = ku_{2x} + \alpha u - \beta u^q$	$u(t, x) = \frac{1}{\left(1 + \exp \left(\frac{x}{\sqrt{6}} - \frac{5t}{6} \right) \right)^2}$	$k = 1.0$, $\alpha = 1.0$, $\beta = 1.0$, $q = 2.0$	$x \in [-40, 40]$ ($n = 401$), $t \in [0, 2]$ ($m = 201$)
Sine-Gordon eq. $u_{2t} = ku_{2x} - \alpha \sin(u)$	$u(t, x) = 4\tan^{-1}(\operatorname{sech}(x)t)$	$k = 1.0$, $\alpha = 1.0$	$x \in [-2, 2]$ ($n = 401$), $t \in [0, 1]$ ($m = 101$)

TABLE III. GEP hyper-parameters selected for identification of various PDEs.

Hyper-parameters	Wave eq.	Heat eq.	Burgers eq. (i)	Burgers eq. (ii)
Head length	2	2	4	2
Number of genes	1	2	1	2
Population size	25	25	20	50
Generations	100	100	500	500
Length of RNC array	10	10	30	5
Random constant minimum	-10	-1	-1	-1
Random constant maximum	10	1	1	1

The GEP hyper-parameters used for identification of wave equation is listed in Table III. We use small number of head length and a single gene for simple cases like liner wave PDE. We note that any other combinations of hyper-parameters may identify the underlying PDE. Fig. 5 illustrates the identified PDE in expression tree (ET) form. When ET form is simplified, we can show that the resulting equation is wave PDE identified with its wave speed parameter a .

TABLE IV. GEP hyper-parameters selected for identification of various PDEs.

Hyper-parameters	KdV eq.	Kawahara eq.	NWS eq.	Sine-Gordon eq.
head length	6	2	5	3
number of genes	5	1	3	2
population size	20	20	30	100
generations	500	100	100	500
length of RNC array	30	5	25	20
random constant minimum	1	-1	-10	-10
random constant maximum	10	1	10	10

TABLE V. GEP functional and terminal set used for equation discovery. ‘?’ is a random constant.

Parameter	Value
Function set	$+, -, \times, /, \sin, \cos$
Terminal set	$\tilde{\Theta}(\mathbf{U}), ?$
Linking function	$+$

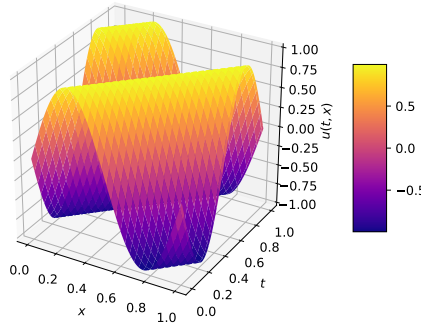


FIG. 4. Analytical solution of wave equation.

The regularization weight (λ) in STRidge is swept across various values as shown Fig. 6. The yellow line in Fig. 6 represents the value of λ at which the best identified PDE is selected. Note that in this simple case STRidge was able to find wave equation for almost all the values of λ 's that are selected. Table VI shows the wave PDE recovered by both GEP and STRidge.

TABLE VI. Wave equation identified by GEP and STRidge.

	Recovered	Test error
True	$u_t = -1.00 u_x$	
GEP	$u_t = -1.00 u_x$	1.72×10^{-28}
STRidge	$u_t = -1.00 u_x$	9.01×10^{-29}

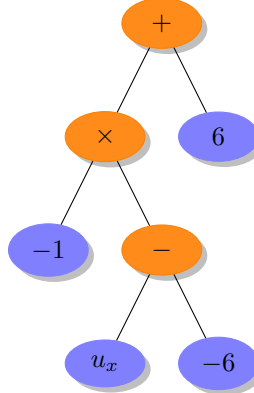


FIG. 5. Wave equation in terms of ET identified by GEP.

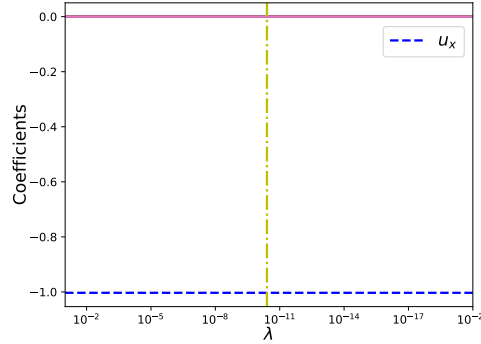


FIG. 6. STRidge coefficients as a function of regularization parameter λ for wave equation.

B. Heat Equation

We use heat equation which is a second order linear PDE to test both SR approaches. The PDE and its analytical solution is listed in Table II. The physical parameter $\alpha = 1.0$ may represent thermal conductivity. Fig. 7 shows the analytical solution $u(t, x)$ of heat equation. Table III show the GEP hyper-parameters used for identification of heat equation. Fig. 8 shows the identified PDE in the form of expression tree (ET). When ET form is simplified, we can show that the resulting model is heat equation identified with its coefficient α .

The regularization weight (λ) in STRidge is swept across various values as shown Fig. 9. The yellow line in Fig. 9 represents the value of λ selected at which STRidge finds heat equation accurately. Note that STRidge was able to find heat equation for low values of regularization weight λ as shown in Fig. 9. Table VII shows the heat equation recovered by both GEP and STRidge. STRidge was able to find more accurate coefficient (α) value than GEP. Furthermore a small constant value is also identified along with heat equation by GEP.

C. Burgers Equation (i)

Burgers equation is a fundamental nonlinear PDE occurring in various areas such as fluid mechanics, nonlinear acoustics, gas dynamics and traffic flow^{69,70}. The interest in

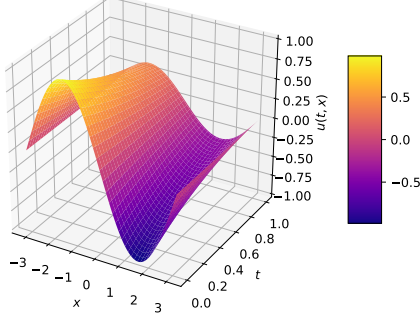


FIG. 7. Analytical solution of heat equation.

TABLE VII. Heat equation identified by GEP and STRidge.

	Recovered	Test error
True	$u_t = -1.00 u_{2x}$	
GEP	$u_t = -0.99 u_{2x} - 5.33 \times 10^{-15}$	5.55×10^{-24}
STRidge	$u_t = -1.00 u_{2x}$	4.09×10^{-30}

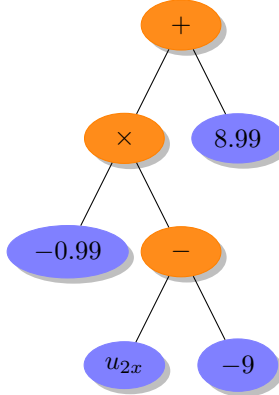


FIG. 8. Heat equation in terms of ET identified by GEP.

Burgers equation arises due to non linear term uu_x and present a challenge to both GEP and STRidge in identification of its PDE using data. The form of the Burgers PDE and its analytical solution⁷¹ is listed in Table II. The physical parameter $\nu = 0.01$ can be considered as kinematic viscosity in fluid flows. Fig. 10 shows the analytical solution $u(t, x)$ of Burgers equation. Table III show the GEP hyper-parameters used for identification of Burgers equation. Fig. 11 shows the identified PDE in the form of expression tree (ET). When ET form is simplified, we can show that the resulting model is Burgers equation identified along with the coefficient of nonlinear term and kinematic viscosity. GEP uses more number of generations for identifying the Burgers PDE due to its nonlinear behaviour along with identification of feature interaction term uu_x .

The regularization weight (λ) in STRidge is swept across various values as shown Fig. 12.

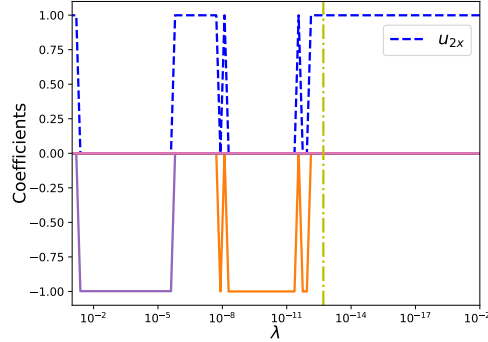
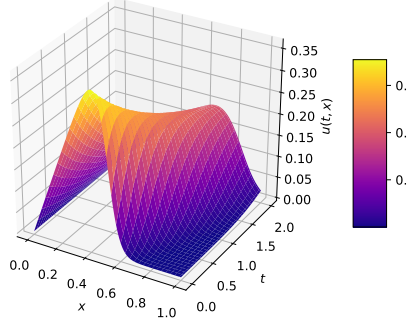
FIG. 9. STRidge coefficients as a function of regularization parameter λ for heat equation.

FIG. 10. Analytical solution of Burgers equation (i).

The yellow line in Fig. 12 represents the value of λ at which the best identified PDE is selected. Note that STRidge was able to find Burgers equation at multiple values of regularization weights λ . Table VIII shows the Burgers PDE recovered by both GEP and STRidge. There is an additional constant coefficient term recovered by GEP. Furthermore the recovery of nonlinear term using limited feature input shows the usefulness of GEP.

TABLE VIII. Burgers equation (i) identified by GEP and STRidge.

	Recovered	Test error
True	$u_t = -uu_x + 0.01 u_{2x}$	
GEP	$u_t = -uu_x + 0.01 u_{2x} - 1.23 \times 10^{-5}$	6.10×10^{-08}
STRidge	$u_t = -uu_x + 0.01 u_{2x}$	5.19×10^{-08}

D. Burgers Equation (ii)

Burgers PDE with different analytical solution is used to test the effectiveness of GEP and STRidge as the input data is changed but represented by same physical law. New analytical solution Burgers equation (ii) is listed in Table II. The physical parameter $\nu = 0.01$ is used

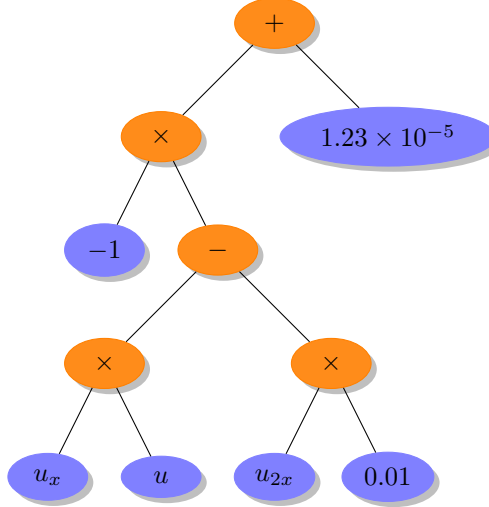


FIG. 11. Burgers equation (i) in terms of ET identified by GEP.

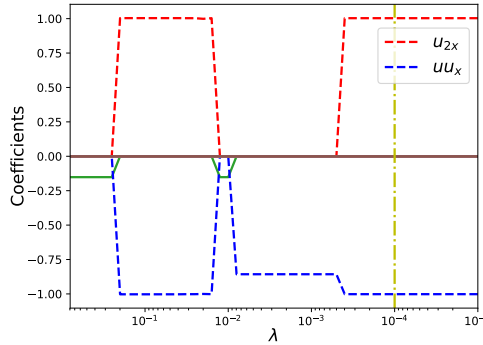


FIG. 12. STRidge coefficients as a function of regularization parameter λ for Burgers equation (i).

to generate the data. Fig. 13 shows the alternate analytical solution $u(t, x)$ of Burgers equation. Table III shows the GEP hyper-parameters used for identification of Burgers equation (ii). Fig. 11 shows the identified PDE in the form of expression tree (ET). When ET form is simplified, we can show that the resulting model is Burgers equation identified along with the coefficient of nonlinear term and kinematic viscosity. With alternate solution, GEP uses more number of head length, genes and population identifying the same Burgers PDE.

The regularization weight (λ) in STRidge is swept across various values as shown Fig. 15. The yellow line in Fig. 15 represents the value of λ at which the best identified PDE is selected. Note that STRidge was able to find Burgers equation at various values of regularization weight λ . Table IX shows the Burgers PDE recovered by both GEP and STRidge.

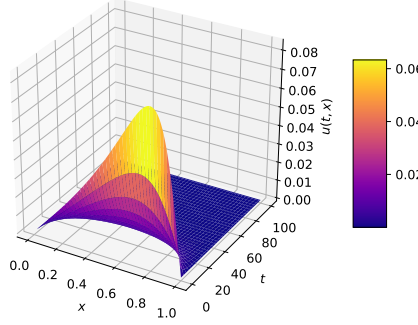


FIG. 13. Analytical solution of Burgers equation (ii).

TABLE IX. Burgers equation (ii) identified by GEP and STRidge.

	Recovered	Test error
True	$u_t = -1.00 uu_x + 0.01 u_{2x}$	
GEP	$u_t = -1.01 uu_x + 0.01 u_{2x} - 3.33 \times 10^{-6}$	1.94×10^{-09}
STRidge	$u_t = -0.99 uu_x + 0.01 u_{2x}$	1.85×10^{-08}

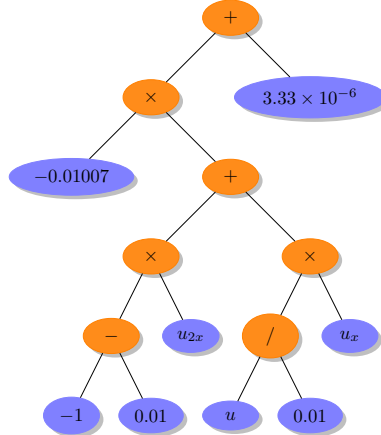


FIG. 14. Burgers equation (ii) in terms of ET identified by GEP.

E. Korteweg-de Vries (KdV) Equation

Korteweg and de Vries derived KdV equation to model Russells phenomenon of solitons^{72,73}. KdV equation also appears when modelling the behavior of magneto-hydrodynamics waves in warm plasma, acoustic waves in an inharmonic crystal and ion-acoustic waves⁷⁴. Many different forms of KdV equation available in the literature but we use the form given in Table II. Fig. 16 shows the analytical solution $u(t, x)$ of KdV equation⁷⁵. It can be seen that this analytical solution refers to two solitons colliding together which forms good test case for SR techniques like GEP and STRidge. Table III show the GEP hyper-parameters used for identification of KdV equation. Due to higher nonlinear dynamics represented

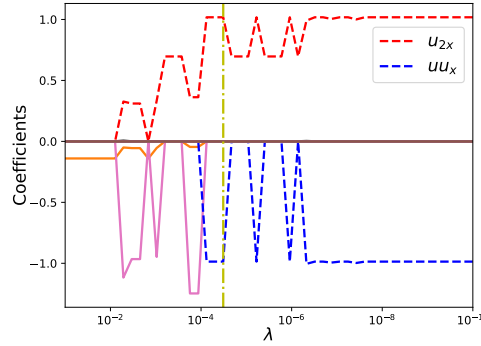


FIG. 15. STRidge coefficients as a function of regularization parameter λ for Burgers equation (ii).

by higher order PDE, GEP requires large head length and genes compared to other test cases in equation discovery. Fig. 17 shows the identified PDE in the form of expression tree (ET). When ET form is simplified, we can show that the resulting model is KdV equation identified along with its coefficients.

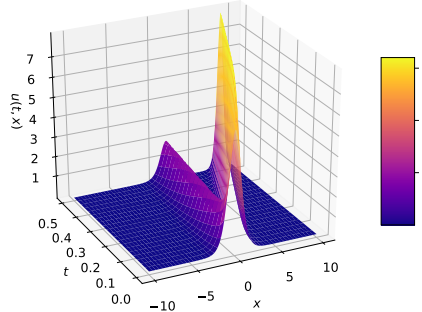


FIG. 16. Analytical solution of KdV equation.

The regularization weight (λ) in STRidge is swept across various values as shown Fig. 18. The yellow line in Fig. 18 represents the value of λ at which the best identified PDE is selected. Note that STRidge was able to find KdV equation at various values of regularization weights (λ). Table X shows the KdV equation recovered by both GEP and STRidge. Physical model identified by STRidge is more accurate to True PDE than model identified by GEP.

TABLE X. KdV equation identified by GEP and STRidge.

	Recovered	Test error
True	$u_t = -6.00 uu_x + 1.00 u_{3x}$	
GEP	$u_t = -5.96 uu_x + 0.99 u_{3x} - 5.84 \times 10^{-4}$	0.29
STRidge	$u_t = -6.04 uu_x + 1.02 u_{3x}$	0.02

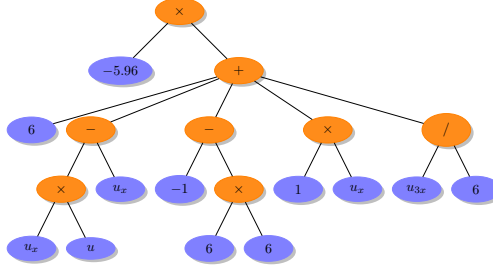
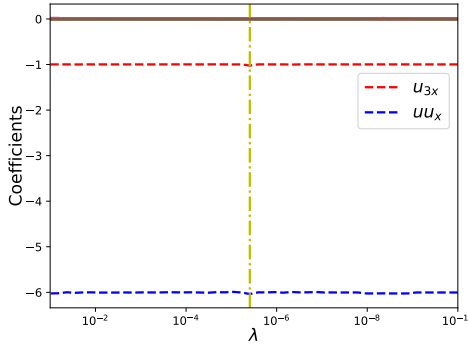


FIG. 17. KdV equation in terms of ET identified by GEP.

FIG. 18. STRidge coefficients as a function of regularization parameter λ for KdV equation.

F. Kawahara Equation

We consider a Kawahara equation which is fifth-order nonlinear PDE⁷⁶ shown in Table II. This equation is sometimes also referred as a fifth-order KdV equation or singularly perturbed KdV equation. The fifth-order KdV equation is one of the most known nonlinear evolution equation which is used in the theory of magneto-acoustic waves in a plasma⁷⁶, capillary-gravity waves⁷⁷ and theory of shallow water waves⁷⁸. This test case is intended to test GEP and STRidge for identifying higher order derivatives from observing data. We use analytical solution⁷⁹ which is a traveling wave soliton given in Table II. This analytical solution also satisfies linear wave equation and hence both GEP and STRidge may recover wave PDE (not show here) as this is the sparsest model represented by observed data. For simplifying the analysis, we remove the potential basis u_x from the feature library⁴¹ ($\Theta(\mathbf{U})$) for STRidge and additionally include uu_x basis in core feature library ($\tilde{\Theta}(\mathbf{U})$) for GEP.

Table III show the GEP hyper-parameters used for identification of Kawahara equation. Due to simplifying the feature library, GEP requires smaller head length and single gene. Fig. 20 shows the identified PDE in the form of expression tree (ET). When ET form is simplified, we can show that the resulting model is Kawahara equation identified along with its coefficients. For STRidge, the regularization weight (λ) is swept across various values as shown Fig. 21. The yellow line in Fig. 21 represents the value of λ at which the best identified PDE is selected. Note that STRidge was able to find Kawahara equation at various values of regularization weights (λ). Table X shows the Kawahara equation identified by both GEP and STRidge.

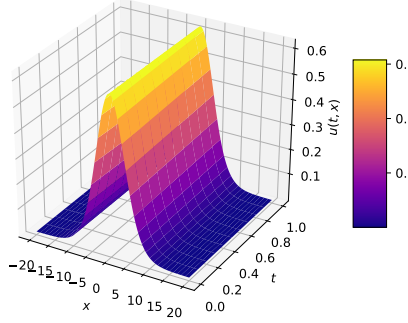


FIG. 19. Analytical solution of Kawahara equation.

TABLE XI. Kawahara equation identified by GEP and STRidge.

	Recovered	Test error
True	$u_t = -1.0 \ uu_x - 1.00 \ u_{3x} - 1.0 \ u_{5x}$	
GEP	$u_t = -1.0 \ uu_x - 1.00 \ u_{3x} - 1.0 \ u_{5x} - 8.27 \times 10^{-8}$	5.29×10^{-11}
STRidge	$u_t = -1.0 \ uu_x - 0.99 \ u_{3x} - 1.0 \ u_{5x}$	1.35×10^{-12}

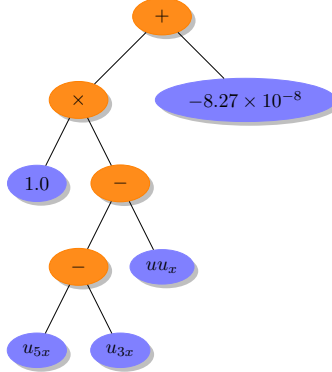


FIG. 20. Kawahara equation in terms of ET identified by GEP.

G. Newell-Whitehead-Segel (NWS) Equation

Newell-Whitehead-Segel equation is a special case of Nagumo equation⁸⁰. Nagumo equation is a nonlinear reaction-diffusion equation that models pulse transmission line simulating a nerve axon⁸¹, population genetics⁸², and circuit theory⁸³. NWS equation and its analytical solution is shown in Table II. We use travelling wave solution⁸⁴ that satisfies both wave and NWS equations. We carry similar changes to feature library that was applied to discovering Kawahara equation.

Table III shows the GEP hyper-parameters used for identification of NWS equation. However contrast to identifying Kawahara equation with smaller head length and single gene from simplifying the feature library, for NWS case GEP requires larger head length and more genes for identifying PDE as shown in Table IV. This is due to identification of

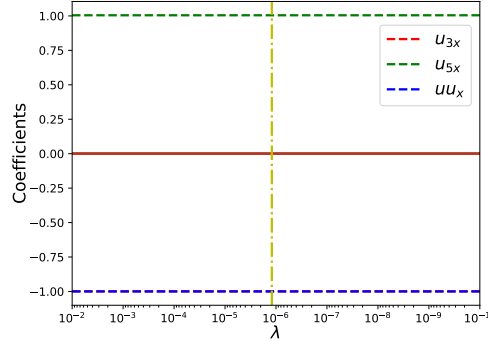
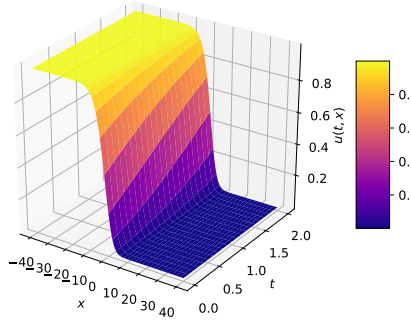
FIG. 21. STRidge coefficients as a function of regularization parameter λ for Kawahara equation.

FIG. 22. Analytical solution of NWS equation.

nonlinear interaction feature u^2 that appear in NWS equation. Fig. 23 shows the identified PDE in the form of expression tree (ET). When ET form is simplified, we can show that the resulting model is NWS equation identified along with its coefficients. For STRidge, the regularization weight (λ) is swept across various values as shown Fig. 24. The yellow line in Fig. 24 represents the value of λ at which the best identified PDE is selected. Note that STRidge was able to find NWS equation at various values of regularization weights (λ). Table X shows the NWS equation identified by both GEP and STRidge.

TABLE XII. NWS equation identified by GEP and STRidge.

	Recovered	Test error
True	$u_t = 1.00 u_{2x} + 1.00 u - 1.00 u^2$	
GEP	$u_t = 0.99 u_{2x} + 0.99 u - 0.99 u^2 - 8.27 \times 10^{-8}$	3.02×10^{-11}
STRidge	$u_t = 1.00 u_{2x} + 0.99 u - 0.99 u^2$	1.36×10^{-11}

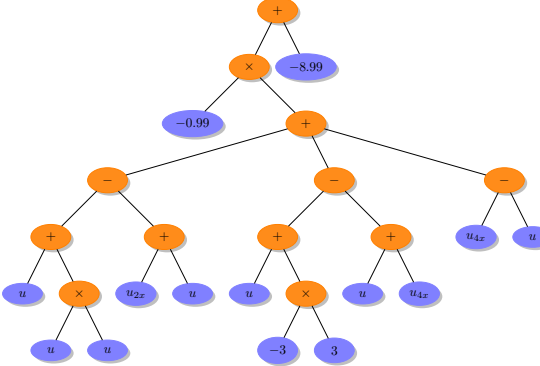
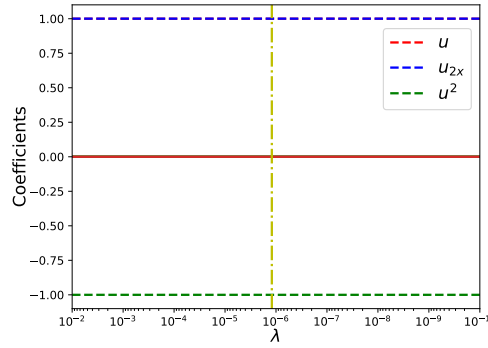


FIG. 23. NWS equation in terms of ET identified by GEP.

FIG. 24. STRidge coefficients as a function of regularization parameter λ for NWS equation.

H. Sine-Gordon Equation

Sine-Gordon equation is a nonlinear PDE that appears in propagating of fluxions in Josephson junctions⁸⁵, dislocation in crystals⁸⁶ and nonlinear optics⁷⁰. Sine-Gordon equation has sine term that needs to be identified by GEP and STRidge by observing data. This test case is straight forward for GEP as the function set includes trigonometric operators that helps to identify the equation. However, application of STRidge is suitable if features library is limited to basic interactions and does not contain basis with trigonometric dependencies. STRidge may recover infinite series approximations if higher degree basic feature interactions are included in feature library³⁸. Note that the output or target data for Sine-Gordon equation consists of second order temporal derivative of velocity field $u(t, x)$. Hence, $\mathbf{V}(t)$ consists of u_{2t} measurements instead of u_t .

Table IV show the GEP hyper-parameters used for identifying the Sine-Gordon equation. For our analysis, GEP found best model when larger population size used. Fig. 26 shows the identified PDE in the form of expression tree (ET). When ET form is simplified, we can show that the resulting model is Sine-Gordon equation identified along with its coefficients. Table XIII shows the identified equation by GEP. This test case shows the usefulness of GEP in identifying models with complex function composition and limitation of expressive and prediction power of feature library in STRidge.

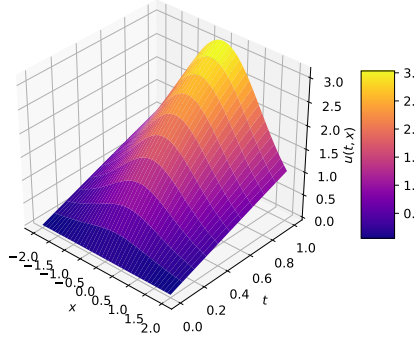


FIG. 25. Analytical solution of Sine-Gordon equation.

TABLE XIII. Sine-Gordon equation identified by GEP.

Recovered	Test error
True $u_{2t} = 1.00 u_{2x} - 1.00 \sin(u)$	
GEP $u_{2t} = 0.99 u_{2x} - 0.99 \sin(u) - 1.82 \times 10^{-5}$	1.57×10^{-4}

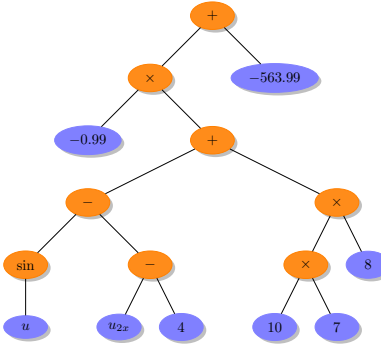


FIG. 26. Sine-Gordon equation in terms of ET identified by GEP.

IV. TRUNCATION ERROR ANALYSIS

This section deals with constructing modified differential equation (MDE) for Burgers equation and demonstrate both GEP and STRidge as SR technique in identification of truncation errors resulting from MDE of Burgers nonlinear PDE. MDEs provide valuable insights of discretization schemes along with their temporal and spatial truncation errors. Initial MDE analysis was developed to connect the stability for nonlinear difference equation with the form of truncation errors⁸⁷. In continuation, symbolic form of MDE was developed and a key insight was proposed that the only first few terms of MDE dominate the properties of the numerical discretization⁸⁸. These developments of MDE analysis lead to increasing accuracy orders by eliminating leading order truncation error terms⁸⁹, improving stability of schemes by adding artificial viscosity terms⁹⁰ and in adaptive mesh refinement⁸⁹. MDE analysis plays a prominent role in implicit large eddy simulation (ILES)⁹¹ as truncation errors are shown to be having inherent turbulence modeling capability⁹². Discretization schemes are tuned in ILES approach to model subgrid scale tensor using truncation errors.

As the construction of MDEA becomes cumbersome and intractable for complex flow configurations, data driven SR tools such as GEP and STRidge can be exploited for identification of MDEs by observing the data.

TABLE XIV. GEP hyper-parameters selected for identification of truncation error terms of MDEs.

Hyper-parameters	Burgere eq. (i)	Burgers eq. (ii)
Head length	8	8
Number of genes	5	4
Population size	70	70
Generations	1000	1000
Length of RNC array	20	20
Random constant minimum	1.0×10^{-6}	1.0×10^{-5}
Random constant maximum	0.01	0.01

For demonstrating purposes, we begin by constructing MDE of Burgers equation,

$$u_t + uu_x = \nu u_{2x}, \quad (14)$$

and discretizing Eq. (14) with first order upwinding scheme (i.e., forward time and backward space approximation for first order spatial and temporal derivatives) and second order accurate central difference approximation for second order spatial derivatives. The resulting discretized Burgers PDE is shown below,

$$\frac{u_j^{p+1} - u_j^{p-1}}{dt} + u_j^p \frac{u_j^p - u_{j-1}^p}{dx} = \nu \frac{u_{j+1}^p - 2u_j^p + u_{j-1}^p}{dx^2}, \quad (15)$$

where temporal and spatial step is given by dt and dx respectively. In Eq. 15, the spatial location is denoted using subscript index j and the temporal snapshot using superscript index p .

To derive modified differential equation (MDE) of Burgers PDE, we substitute Taylor approximations for each term,

$$\left. \begin{aligned} u_j^{p+1} &= u_j^p + dt(u_t)_j^p + \frac{dt^2}{2}(u_{2t})_j^p + \frac{dt^3}{6}(u_{3t})_j^p + \dots \\ u_{j+1}^p &= u_j^p + dx((u_t))_j^p + \frac{dx^2}{2}(u_{2x})_j^p + \frac{dx^3}{6}(u_{3x})_j^p + \dots \\ u_{j-1}^p &= u_j^p - dx(u_x)_j^p + \frac{dx^2}{2}(u_{2x})_j^p - \frac{dx^3}{6}(u_{3x})_j^p + \dots \end{aligned} \right\} \quad (16)$$

We substitute these developments in Eq. 15, obtaining Burgers MDE,

$$(u_t + uu_x - \nu u_{2x})_j^p = -R, \quad (17)$$

where R is truncation error terms of Burgers MDE given as,

$$R = \frac{dt}{2}(u_{2t})_j^p + \frac{dx}{2}(uu_x)_j^p - \frac{\nu dx^2}{12}(u_{4x})_j^p + O(dt^2, dx^4) \quad (18)$$

Furthermore, temporal derivative in Eq. 18 is substituted with spatial derivatives resulting in,

$$\begin{aligned} R &= dtuu_x^2 - dt\nu u_x u_{2x} - dt\nu uu_{3x} \\ &\quad - \frac{dx}{2}uu_{2x} + \frac{dt}{2}u^2 u_{2x} - \frac{\nu dx^2}{12}u_{4x} + O(dt^2, dx^4) \end{aligned} \quad (19)$$

The truncation error or residual of discretized equation considering $u(t, x)$ as exact solution to Burgers PDE is equal to difference between the numerical scheme (Eq. 15) and differential equation (Eq. 14)⁹³. This results in discretized equation with residual as shown below,

$$u_j^{p+1} - u_j^{p-1} + u_j^p dt \frac{u_j^p - u_{j-1}^p}{dx} - \nu dt \frac{u_{j+1}^p - 2u_j^p + u_{j-1}^p}{dx^2} = Rdt. \quad (20)$$

We follow the same methodology for constructing output data and feature library as discussed in Section II for equation discovery. However the output or target data $\mathbf{V}(\mathbf{t})$ is stored with the left hand side of Eq. 20 denoted from now as \mathbf{u}_{er} . The resulting output and core feature library is shown below,

$$\left. \begin{aligned} \mathbf{V}(\mathbf{t}) &= [\mathbf{U}_{er}] \\ \tilde{\Theta}(\mathbf{U}) &= [\mathbf{U} \ \mathbf{U}_x \ \mathbf{U}_{2x} \ \mathbf{U}_{3x} \ \mathbf{U}_{4x}] \end{aligned} \right\} \quad (21)$$

The computation of output data $\mathbf{V}(\mathbf{t})$ in Eq. 21 can be obtained using analytical solution $u(t, x)$ of Burgers PDE. Furthermore, the derivatives in core feature library $\tilde{\Theta}(\mathbf{U})$ is calculated using finite difference approximations given by Eq. 4. We use both analytical solution $u(t, x)$ listed in Table II for Burgers equation (i) and Burgers equation (ii) to test GEP and STRidge for recovering truncation error terms.

We use the same extended feature library $\tilde{\Theta}(\mathbf{U})$ as input to STRidge given in Eq. 7 but without fifth order derivatives. However we add additional third degree interaction of features to $\tilde{\Theta}(\mathbf{U})$ so as to recover the truncation error terms containing third degree nonlinearity. The extra nonlinear features that are added to $\tilde{\Theta}(\mathbf{U})$ are given below,

$$\begin{aligned} &[\mathbf{U}^2 \mathbf{U}_x \ \mathbf{U}^2 \mathbf{U}_{2x} \ \mathbf{U}^2 \mathbf{U}_{3x} \ \mathbf{U}^2 \mathbf{U}_{4x} \\ &\quad \mathbf{U} \mathbf{U}_x^2 \ \mathbf{U} \mathbf{U}_x \mathbf{U}_{2x} \ \mathbf{U} \mathbf{U}_x \mathbf{U}_{3x} \ \mathbf{U} \mathbf{U}_x \mathbf{U}_{4x}]. \end{aligned}$$

In contrast, GEP uses the core feature $\tilde{\Theta}(\mathbf{U})$ as input as it tries to identify the higher order nonlinear feature interactions automatically. This test case shows the natural feature extraction capability of GEP and modification of feature library so as to increase the expressive power of STRidge.

TABLE XV. GEP functional and terminal set used for truncation error term recovery. ‘?’ is a random constant.

Parameter	Value
Function set	+, -, ×
Terminal set	$\tilde{\Theta}(\mathbf{U})$, ?
Linking function	+

The functional and terminal set used for truncation error identification is listed in Table XV. First we test the recovery of truncation errors using analytical solution of Burgers equation (i) with same spatial and temporal domain listed in Table II. However, we set spatial discretization to be $dx = 0.005$ and temporal discretization to $dt = 0.005$ for storing the analytical solution $u(t, x)$. This test case needed large population size, bigger head length, more number of genes and iterations given in Table XIV as the truncation error terms consists of nonlinear combinations of features and the coefficients of error terms that are generally difficult for GEP to identify. Fig. 27 shows the ET form of identified truncation error terms. The regularization weight λ for STRidge is swept across a range of values

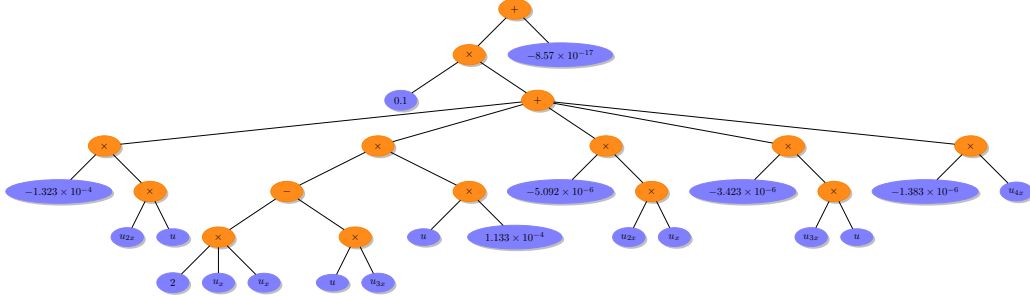


FIG. 27. Truncation error of Burgers MDE using analytical solution of Burgers equation (i) in terms of ET identified by GEP.

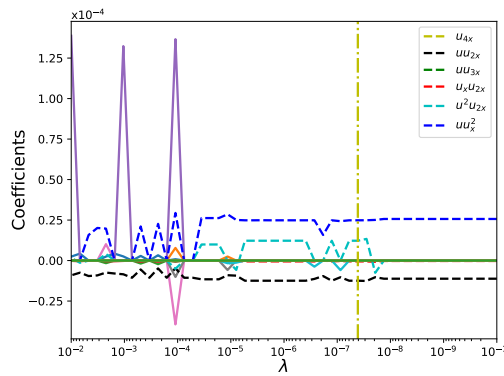


FIG. 28. STRidge coefficients as a function of regularization parameter λ for truncation error of Burgers MDE (i).

as shown in Fig. 28. The vertical yellow line in Fig. 28 is the value of λ where STRidge identifies best truncation error model. Table XVI shows the recovered error terms by GEP and STRidge along with their coefficients. Both GEP and STRidge perform well in identifying the nonlinear spatial error terms with STRidge predicting the error coefficient better than GEP.

In the second case, we test the recovery of truncation errors using analytical solution of Burgers eq. (ii) with same spatial and temporal domain listed in Table II. We select spatial discretization $dx = 0.005$ and temporal discretization $dt = 0.1$ for propagating the analytical solution $u(t, x)$. This test case also follows the previous case where large population size, bigger head length, more number of genes and iterations are needed as shown in Table XIV. Fig. 29 shows the ET form of identified truncation error terms. The regularization weight λ for STRidge is swept across a range of values as shown in Fig. 28. In this test case, the coefficients with λ change rapidly and best model is recovered only at the value of λ shown by vertical yellow line in Fig. 28. Table XVII shows the recovered error terms by GEP and STRidge along with their coefficients. Similar to previous test case, truncation error coefficients are better predicted by STRidge than GEP.

V. HIDDEN PHYSICS DISCOVERY

In this section we demonstrate the identification of hidden physical laws from sparse data mimicking sensor measurements using GEP and STRidge. Furthermore, we demonstrate the usefulness of GEP as natural feature extractor capable for identifying complex functional

TABLE XVI. Identified truncation error terms along with coefficients for Burgers MDE (i) by GEP and STRidge.

	True	GEP	Relative error (%)	STRidge	Relative error (%)
uu_x^2	2.5×10^{-5}	2.26×10^{-5}	9.6	2.48×10^{-5}	0.8
$u_x u_{2x}$	-5.0×10^{-7}	-5.09×10^{-7}	1.8	-5.02×10^{-7}	0.4
uu_{3x}	-2.5×10^{-7}	-3.42×10^{-7}	36.8	-2.29×10^{-7}	8.4
$u^2 u_{2x}$	1.25×10^{-5}	1.13×10^{-5}	9.6	1.22×10^{-5}	2.4
u_{4x}	1.25×10^{-9}	1.38×10^{-9}	10.4	1.16×10^{-9}	7.2
uu_{2x}	-1.25×10^{-5}	-1.33×10^{-5}	6.4	-1.24×10^{-5}	0.8

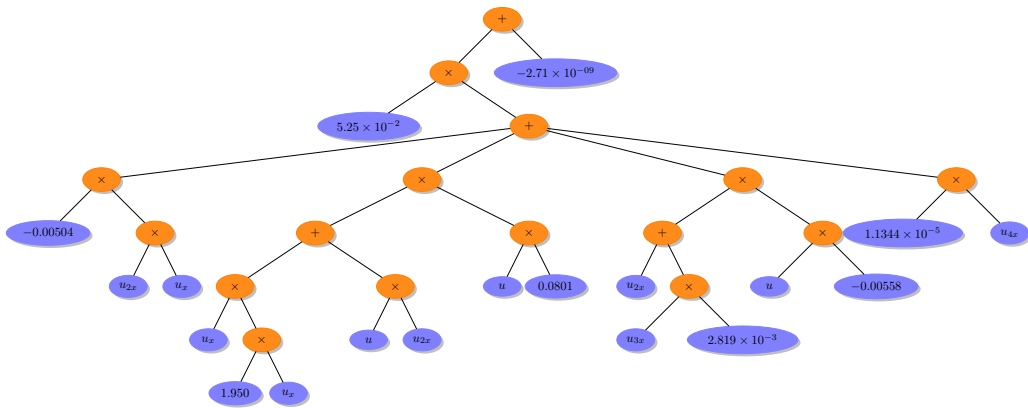


FIG. 29. Truncation error term Burgers MDE using analytical solution of Burgers equation (ii) in terms of ET identified by GEP.

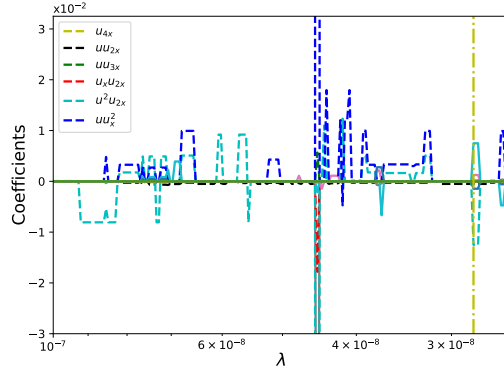


FIG. 30. STRidge coefficients as a function of regularization parameter λ for truncation error of Burgers MDE (ii).

compositions while STRidge in its current form is limited by its expressive power which depends on its input feature library. Many governing equations of complex systems in modern world are only partially known or in some cases still awaiting for first principle equations. For example, full atmospheric radiation models or chemical reaction models are not known in governing equations of environmental systems^{94,95}. These unknown models generally manifested in right hand side of known governing equations behaving as source or

TABLE XVII. Identified truncation error terms along with coefficients for Burgers MDE (ii) by GEP and STRidge.

	True	GEP	Relative error (%)	STRidge	Relative error (%)
uu_x^2	1.0×10^{-2}	8.19×10^{-3}	18.1	9.92×10^{-3}	0.8
$u_x u_{2x}$	-2.0×10^{-4}	-2.64×10^{-4}	32.0	-1.99×10^{-4}	0.5
uu_{3x}	-1.0×10^{-4}	-1.55×10^{-4}	55.0	-9.91×10^{-5}	0.9
$u^2 u_{2x}$	5.0×10^{-3}	4.21×10^{-3}	15.8	5.08×10^{-3}	1.6
u_{4x}	5.0×10^{-7}	5.65×10^{-7}	13.0	4.94×10^{-7}	1.2
uu_{2x}	-2.5×10^{-4}	-2.75×10^{-4}	10	-2.54×10^{-4}	1.6

forcing term for a dynamical system. Recent explosion of rapid data gathering using smart sensors⁹⁶ with low cost has enabled researchers to collect data that represent true physics of complex systems but their governing equations being known partially. To this end, SR approaches might be able to recover this unknown physical models when exposed to data representing full physics.

To demonstrate proof of concept for identification of unknown physics, we formulate 1D advection-diffusion PDE and 2D vortex-merger problem with a source term that represents the hidden physical law. We generate synthetic data that contains true physics and use this true data to be substituted in known governing equations. This results in unknown physical model left as a residual that must be recovered by GEP when exposed to target or output containing known governing equations. Furthermore, both GEP and STRidge are tested to recover eddy viscosity kernels for 2D Kraichnan turbulence problem. These eddy viscosity kernels are manifested as source terms in LES governing equations that model unresolved small scales. Additionally, the value of ad-hoc free modelling parameter that controls the dissipation in eddy viscosity models is also recovered using GEP and STRidge.

TABLE XVIII. GEP hyper-parameters selected for identifying source terms for 1D advection-diffusion and 2D vortex-merger problem.

Hyper-parameters	1D advection-diffusion eq.	2D vortex-merger problem
head length	6	5
number of genes	2	3
population size	50	50
generations	1000	500
length of RNC array	5	8
random constant minimum	$\frac{\pi}{4}$	$-\pi$
random constant maximum	π	π

A. 1D Advection-Diffusion PDE

In the first test case, we consider 1D non-homogeneous advection-diffusion PDE which appears in many areas such as fluid dynamics⁹⁷, heat transfer⁹⁸, and mass transfer⁹⁹. The non-homogeneous PDE takes the form,

$$u_t + cu_x = \alpha u_{2x} + S(t, x), \quad (22)$$

where $c = \frac{1}{3\pi}$, $\alpha = \frac{1}{4}$ and $S(t, x)$ being the source term.

We use analytical solution $u(t, x)$ for solving Eq. 22. The exact solution for this non-homogeneous PDE takes the form,

$$u(t, x) = \exp\left(\frac{\pi^2 t}{4}\right) \sin(\pi x), \quad (23)$$

where spatial domain $x \in [0, 1]$ and temporal domain $t \in [0, 1]$. We discretize space and time domains with $n = 501$ and $m = 1001$ respectively. Fig. 31 shows the corresponding analytical solution $u(t, x)$.

The source term $S(t, x)$ which satisfies Eq. 22 for analytical solution in Eq. 23 given as,

$$S(t, x) = \frac{\pi^2}{2} \exp\left(\frac{\pi^2 t}{4}\right) \sin(\pi x) + \frac{1}{3} \exp\left(\frac{\pi^2 t}{4}\right) \cos(\pi x). \quad (24)$$

Our goal is to recover this hidden source term once the solution $u(t, x)$ is available either by solving analytical equation given by Eq. 23 or by sensor measurements in real world applications. Furthermore, we select 64 randomly sparse spatial locations to mimic experimental data collection. After the solution $u(t, x)$ is stored at selected sparse spatial locations, we follow same procedure for constructing output data and feature building as discussed in Section II. The corresponding output data \mathbf{V} and feature library for recovering source term using GEP is given as,

$$\left. \begin{aligned} \mathbf{V} &= \left[\mathbf{U}_t + \mathbf{cU}_x - \alpha \mathbf{U}_{2x} \right] \\ \tilde{\Theta} &= [x \ t] \end{aligned} \right\} \quad (25)$$

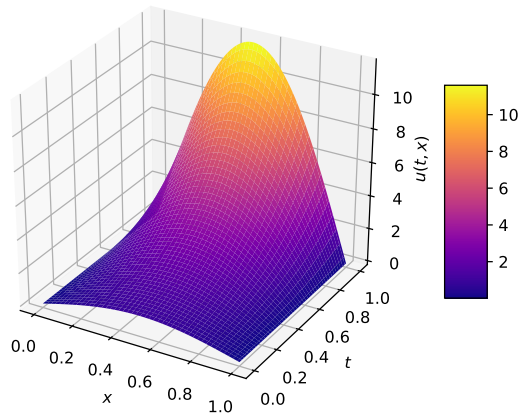


FIG. 31. Solution to 1D advection-diffusion PDE with source term.

The derivatives in the output data \mathbf{V} are calculated using Eq. 4. Hence, to calculate spatial derivatives, we also store additional stencil data $u(t, x)$ around randomly selected sparse location $(u)_j^p$ i.e., $(u)_{j+1}^p, (u)_{j-1}^p$. Table XIX gives the functional and terminal set used by GEP to recover the source term $S(t, x)$ given in Eq. 24.

Table XVIII lists the hyper-parameters used by GEP for recovering source term of 1D advection-diffusion equation. As the hidden physical law given in Eq. 24 consists of complex functional compositions, GEP requires larger head length and more number of generations

TABLE XIX. GEP functional and terminal set used for source term identification. ‘?’ is a random constant.

Parameter	Value
Function set	$+, -, \times, /, \exp, \sin, \cos$
Terminal set	$\tilde{\Theta}, ?$
Linking function	$+$

required by GEP to identify. The ET form of the source term $S(t, x)$ found by GEP is shown in Fig. 32. The identified source term after simplifying the ET form found by GEP is listed in Table XX. GEP was able to identify the source term $S(t, x)$ given in Eq. 24 from sparse data.

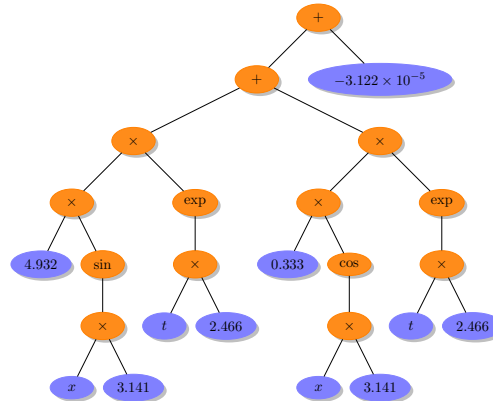


FIG. 32. Hidden source term of 1D advection-diffusion PDE in terms of ET identified by GEP.

TABLE XX. Hidden source term (S) of 1D advection-diffusion PDE identified by GEP.

	Recovered	Test error
True	$S = 4.93 \exp(2.47 t) \sin(3.14 x) + 0.33 \exp(2.47 t) \cos(3.14 x)$	
GEP	$S = 4.93 \exp(2.46 t) \sin(3.14 x) + 0.33 \exp(2.46 t) \cos(3.14 x) - 3.12 \times 10^{-5}$	3.34×10^{-7}

B. 2D Vortex-Merger Problem

In this section we demonstrate the recovery of hidden physical law from the data generated by solving vortex-merger problem with source term. The initial two vortices merge to form a single vortex when they are located within a certain critical distance from each other. This two-dimensional process is one of the fundamental processes of fluid motion and it plays a key role in a variety of simulations, such as decaying two-dimensional turbulence¹⁰⁰, three-dimensional turbulence¹⁰¹, and mixing layers¹⁰². This phenomenon also occurs in other fields such as astrophysics, meteorology, and geophysics¹⁰³. Vortex-merger problem is simulated by using 2D incompressible Navier-Stokes equations for the domain with periodic boundary condition.

We specifically solve system of PDEs called vorticity-streamfunction formulation. This system of PDEs contain vorticity transport equation derived from taking curl of 2D incom-

pressible Navier-Stokes equations and Poisson equation representing kinematic relationship between the streamfunction (ψ) and vorticity (ω). The resulting vorticity-streamfunction formulation with source term is given as,

$$\left. \begin{aligned} \omega_t + J(\omega, \psi) &= \frac{1}{\text{Re}} \nabla^2 \omega + S(t, x, y), \\ \nabla^2 \psi &= -\omega, \end{aligned} \right\} \quad (26)$$

where Reynolds number of flow taken as $\text{Re} = 2000$. In Eq. 26, $S(t, x, y)$ is the source term and $J(\omega, \psi)$ is Jacobian term given as $\psi_y \omega_x - \psi_x \omega_y$. We use Cartesian domain $(x, y) \in [0, 2\pi] \times [0, 2\pi]$ with spatial resolution of 128×128 . The initial vorticity field of merging, co-rotating vortex pair is generated using superposition of two Gaussian-distributed vortices given by,

$$\begin{aligned} \omega(0, x, y) = \Gamma_1 \exp & \left(-\rho \left[(x - x_1)^2 + (y - y_1)^2 \right] \right) \\ & + \Gamma_2 \exp \left(-\rho \left[(x - x_2)^2 + (y - y_2)^2 \right] \right), \end{aligned} \quad (27)$$

where circulation $\Gamma_1 = \Gamma_2 = 1$, interacting constant $\rho = \pi$ and the intial vortex centers located near each other with coordinates $(x_1, y_1) = (\frac{3\pi}{4}, \pi)$ and $(x_2, y_2) = (\frac{5\pi}{4}, \pi)$. We choose the source term $S(t, x)$ as,

$$S(t, x, y) = \Gamma_0 \sin(x) \cos(y) \exp \left(\frac{-4\pi^2}{\text{Re}} t \right), \quad (28)$$

where magnitude of source $\Gamma_0 = 0.01$.

The vorticity ω field and streamfunction ψ field is obtained by solving the Eq. 26 numerically. We use third-order Runge-Kutta numerical scheme for the time integration and second order Arakawa scheme¹⁰⁴ for the discretization of Jacobian term $J(\omega, \psi)$ and vorticity diffusion term. As we have periodic domain, we use fast Fourier transform (FFT) for solving Poisson equation in Eq. 26 to get streamfunction at every time step. Specific algorithm and numerical details for solving vortex-merger problem can be found at San et al^{102,105}. We integrate the solution from time $t = 0$ to $t = 20$ with temporal step $dt = 0.01$.

Fig. 33 shows the merging process of two vortices at initial and final time. The red markers in Fig. 33 are 64 randomly selected sparse locations to collect both streamfunction ψ and vorticity ω data. Once the streamfunction ψ and vorticity ω data at sparse locations are available, we construct the target data \mathbf{V} and feature library $\tilde{\Theta}$ as discussed in Section II. The resulting input-response data is given as,

$$\left. \begin{aligned} \mathbf{V} &= \left[\omega_t + J(\omega, \psi) - \nabla^2 \omega_{2x} \right], \\ \tilde{\Theta} &= \left[\mathbf{x} \ \mathbf{y} \ \mathbf{t} \right]. \end{aligned} \right\} \quad (29)$$

The derivatives in output data $\mathbf{V}(\mathbf{t})$ are calculated using finite difference approximation similar to Eq. 4. As streamfunction $(\psi)_{j,i}^p$ and vorticity $(\omega)_{j,i}^p$ data are selected only at sparse spatial locations, we also store surrounding stencil i.e., $(\psi)_{j+1,i}^p, (\psi)_{j-1,i}^p, (\psi)_{j,i+1}^p, (\psi)_{j,i-1}^p$ and $(\omega)_{j+1,i}^p, (\omega)_{j-1,i}^p, (\omega)_{j,i+1}^p, (\omega)_{j,i-1}^p$ to calculate the derivatives. The index j represents spatial location in x direction and i represents spatial location in y direction.

In this test case, we demonstrate the identification of hidden physics which is the source term $S(t, x, y)$ given by Eq. 28 from the data obtained at sparse spatial locations using GEP. Table XVIII lists the hyper-parameter used by GEP to recover the hidden physical law. We use same function and terminal set as shown in Table XIX but \times is used as linking function. Fig. 34 shows the ET form of hidden physical law (source term) obtained by GEP. Simplification of the ET form shows the identified source term which is close to true source term as shown in Table XXI.

The 1D advection-diffusion and 2D vortex-merger problem demonstrates the usefulness of GEP in recovering hidden physics i.e., source term that compose of complex functions

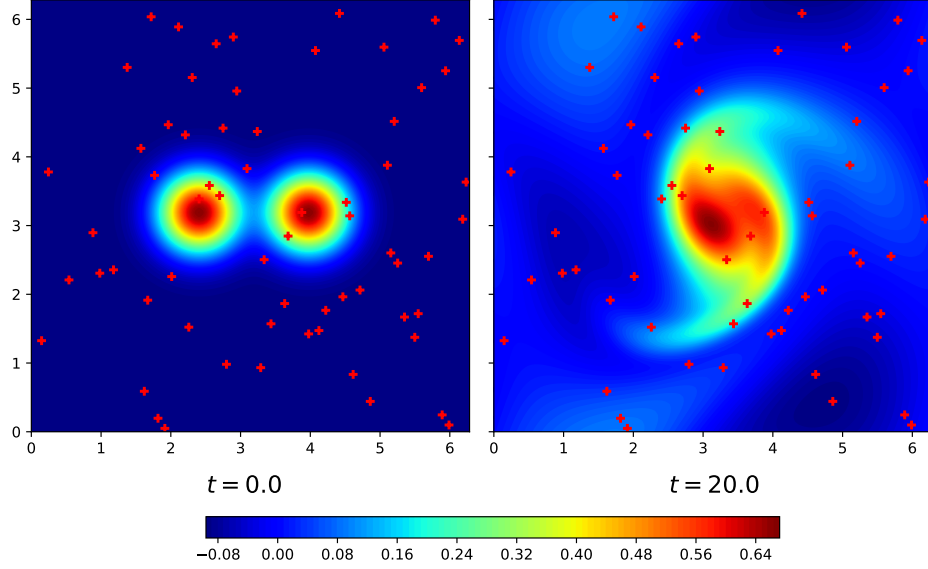


FIG. 33. 2D vortex-merger problem with source term at time $t = 0.0$ and $t = 20.0$. The red markers shows 64 random sensor locations used to collect vorticity (ω) and streamfunction (ψ) data for recovering source term $S(t, x, y)$.

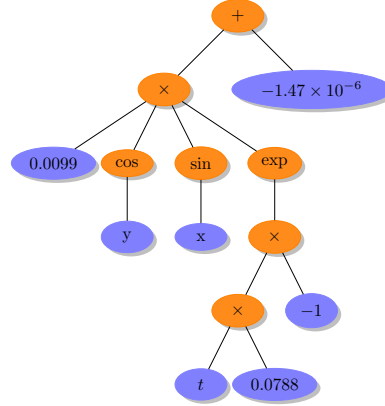


FIG. 34. Hidden source term of 2D vortex-merger problem in terms of ET identified by GEP.

TABLE XXI. Hidden source term (S) of 2D vortex-merger problem identified by GEP.

	Recovered	Test error
True	$S = 0.0100 \sin(x) \cos(y) \exp(-0.078 t)$	
GEP	$S = 0.0099 \sin(x) \cos(y) \exp(-0.078 t) - 1.47 \times 10^{-6}$	1.35×10^{-8}

using randomly selected sparse data. The expressive power of feature library limits the applications of STRidge for identifying complex composition models. However STRidge might be able to identify the infinite series approximations of these nonlinear functions³⁸. In the next test case we use both STRidge and GEP to identify eddy viscosity kernels along with their modelling coefficient, that controls the dissipation of these kernels.

C. 2D Kraichnan Turbulence

The concept of two-dimensional turbulence helps in understanding many complex physical phenomenon such as geophysical and astrophysical flows^{106,107}. Two-dimensional turbulence can treat idealised flow configuration restricted to two-dimensions such as flows in rapidly rotating systems and in thin films over rigid bodies. The physical mechanism associated with two-dimensional turbulence is explained by Kraichnan-Batchelor-Leith (KBL) theory^{108–110}. Generally large eddy simulation (LES) is performed for both two and three dimensional flows to avoid the resolution and thereby computational requirement of direct numerical simulation (DNS)^{111,112}. In LES, flow variables are decomposed into resolved low wave number (or large scale) and unresolved high wavenumber (or small scale). This is achieved by application of low pass spatial filter to flow variables. By arresting high wavenumber content (small scales), we are able to reduce the high resolution requirement of DNS and hence faster simulations and reduced storage requirements. However, the procedure of introducing low pass filtering results in an unclosed term of LES governing equations representing the finer scale effects in the form of source term.

Thus the quality of LES depends on modelling approach to close the spatial filtered governing equations to capture the effects of unresolved finer scales¹¹³. This model also called sub grid scale model is critical part of LES simulations. Functional or eddy viscosity approach is one of the popular approach to model this closure term. These approaches propose an artificial viscosity to mimic the dissipative effect of fine scales. Some of the popular functional models are Smagorinsky model¹¹⁴, Leith model¹¹⁵, Baldwin-Lomax¹¹⁶ and Cebeci-Smith model¹¹⁷. All these models require the need to specify a model constant that controls the quantity of dissipation in the simulation and its value is set based on the encountered flow. In this section we demonstrate the identification of eddy viscosity kernel (model) along with its ad-hoc model constant from observing the source term of LES equation using both GEP and STRidge as SR tools. To this end, we use vorticity-streamfunction formulation for two-dimensional fluid flow given in Eq. 26. We derive the LES equations for two dimensional turbulence by passing low pass spatial filter to vorticity-streamfunction PDE given in Eq. 26. The resulting filtered equation is given as,

$$\bar{\omega}_t + J(\bar{\psi}, \bar{\omega}) = \frac{1}{Re} \nabla^2 \bar{\omega}, \quad (30)$$

where Re is Reynolds number of the flow and $J(\omega, \psi)$ is Jacobian term given as $\psi_y \omega_x - \psi_x \omega_y$. Furthermore the Eq. 30 is rearranged as,

$$\bar{\omega}_t + J(\bar{\psi}, \bar{\omega}) = \frac{1}{Re} \nabla^2 \bar{\omega} + \Pi, \quad (31)$$

where LES source term Π is given as,

$$\Pi = J(\bar{\psi}, \bar{\omega}) - \bar{J}(\psi, \omega). \quad (32)$$

This source term Π in Eq. 32 represents the influence of the subgrid scales on large resolved scales. The term $\bar{J}(\psi, \omega)$ is not available which necessitates the use of closure modelling approach. In functional or eddy viscosity models, the source term of LES equations is represented as,

$$\Pi = \nu_e \nabla^2 \bar{\omega}. \quad (33)$$

where eddy viscosity ν_e is given by but not limited to Smagorinsky kernel, Leith kernel and Baldwin-Lomax kernel and Cebeci-Smith kernel. The choice of these eddy viscosity kernels essentially implies the choice of a certain function of local field variable such as strain rate or gradient of vorticity as a control parameter for the magnitude of ν_e .

In Smagorinsky model, the eddy viscosity kernel is given by,

$$\nu_e = (c_s \delta)^2 |\bar{S}|, \quad (34)$$

TABLE XXII. GEP functional and terminal set used for identifying eddy viscosity kernel. ‘?’ is a random constant.

Parameter	Value
Function set	$+, -, \times, /$
Terminal set	$\tilde{\Theta}, ?$
Linking function	+

where c_s is free modelling constant that controls magnitude of dissipation and δ is a characteristic grid length scale given by square root of product of cell sizes in each directions. The $|\bar{S}|$ is based on second invariant of filtered field deformation and given by,

$$|\bar{S}| = \sqrt{4\bar{\psi}_{xy}^2 + (\bar{\psi}_{2x} - \bar{\psi}_{2y})^2}, \quad (35)$$

The Leith model proposes the eddy viscosity kernel as a function of vorticity given as,

$$\nu_e = (c_s \delta)^3 |\nabla \bar{\omega}|, \quad (36)$$

where $|\nabla \bar{\omega}|$ controls the dissipative characteristic of eddy viscosity as against resolved strain rate used in Smagorinsky model. The magnitude of gradient of vorticity is defined as,

$$|\nabla \bar{\omega}| = \sqrt{\bar{\omega}_x^2 + \bar{\omega}_y^2}. \quad (37)$$

TABLE XXIII. GEP hyper-parameters selected for identification of eddy viscosity kernel for Kraichnan turbulence.

Hyper-parameters	Kraichnan turbulence
Head length	2
Number of genes	2
Population size	20
Generations	500
Length of RNC array	3
Random constant minimum	-1
Random constant maximum	1

Baldwin-Lomax is an alternative approach that models eddy viscosity kernel as,

$$\nu_e = (c_s \delta)^2 |\bar{\omega}|, \quad (38)$$

where $|\bar{\omega}|$ is absolute value of vorticity considered as measure of local energy content of the flow at a grid point and also a measure of dissipation required at that location.

Cebeci-Smith model was devised for Reynolds Averaged Navier-Stokes (RANS) applications. The model is modified for LES applications and given as,

$$\nu_e = (c_s \delta)^2 |\bar{\Omega}|, \quad (39)$$

where $|\bar{\Omega}|$ is given as,

$$|\bar{\Omega}| = \sqrt{\bar{\psi}_{2x}^2 + \bar{\psi}_{2y}^2}. \quad (40)$$

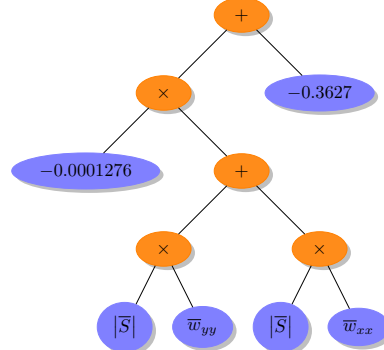


FIG. 35. Smagorinsky kernel in terms of ET identified for two-dimensional Kraichnan turbulence problem by GEP.

TABLE XXIV. LES source term (Π) for two-dimensional Kraichnan turbulence problem identified by GEP and STRidge.

Recovered	
GEP	$\Pi = 0.000128 S w_{2x} + 0.000128 S w_{2y} - 0.362$
STRidge	$\Pi = 0.000132 S w_{2x} + 0.000129 S w_{2y}$

High fidelity DNS simulations are performed for Eq. 30. We use square domain of length 2π with periodic boundary conditions in all directions. We specifically simulate homogeneous isotropic decaying turbulence which may be specified by an initial energy spectrum which decays through time. High fidelity DNS simulations are carried for $Re = 4000$ with 1024×1024 resolution from time $t = 0$ to $t = 4.0$ with time step 0.001. The filtered flow quantities and LES source term Π in Eq. 32 is obtained from coarsening the DNS quantities to obtain quantities with 64×64 resolution. The details of solver and coarsening can be referred to San and Staples¹⁰¹. Once the LES source term Π in Eq. 32 and filtered flow quantities are obtained, we build feature library and output data similar to the discussion in Section II. The resulting input-response data is given as,

$$\begin{aligned} \mathbf{V} &= [\Pi] \\ \tilde{\Theta} &= [\bar{\omega}_{2x} \bar{\omega}_{2y} |\bar{S}| |\nabla \bar{\omega}| |\bar{\omega}| |\bar{\Omega}|] \end{aligned} \quad (41)$$

GEP uses the output and feature library given in Eq. 41 to automatically extract best eddy viscosity kernel for decaying turbulence problem along with the models ad-hoc coefficient.

The extended feature library is constructed to include nonlinear interaction upto quadratic degree to expand the expressive power for STRidge algorithm. The resulting extended feature library is given as,

$$\Theta = [1 \bar{\omega}_{2x} \bar{\omega}_{2x}^2 \bar{\omega}_{2y} \bar{\omega}_{2x} \bar{\omega}_{2y} \bar{\omega}_{2y}^2 \dots |\bar{\Omega}|^2]. \quad (42)$$

The function and terminal set used for identification of eddy viscosity kernel by GEP is listed in Table XXII. Furthermore, the hyper-parameters of GEP are listed in Table XXIII. Both GEP and STRidge identifies Smagorinsky kernel with approximately same coefficients as shown in Table XXIV. The ET form of Smagorinsky kernel found by GEP is shown in Fig. 35. The regularization weight λ is varied for various values to recover multiple models of different complexity as shown in Fig. 36. The yellow line in Fig. 36 corresponds to the value

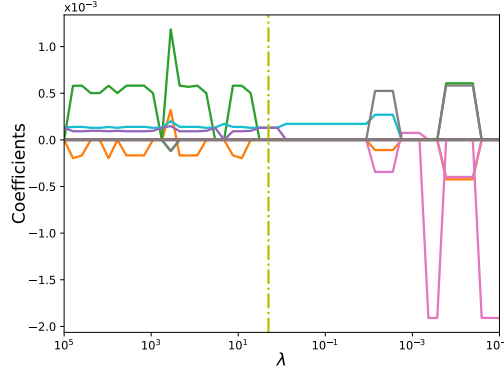


FIG. 36. STRidge coefficients as a function of regularization parameter λ for two-dimensional Kraichnan turbulence problem.

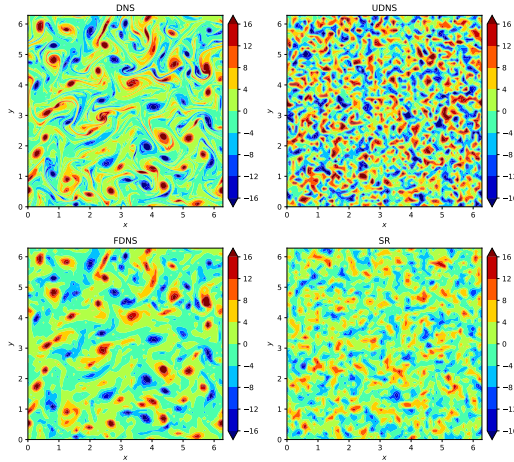


FIG. 37. Contour plots for two-dimensional Kraichnan turbulence problem at $t = 4$. SR refers to the identified model of the Smagorinsky kernel with $c_s = 0.12$. UDNS and FDNS refer to the no-model and filtered DNS simulations, respectively.

of λ where STRidge identifies Smagorinsky kernel. We can take average coefficient from both SR tools and derive the value of free modelling constant identified by SR approaches. The average model of both approaches is given by,

$$\Pi = 0.000129 (|S| w_{2x} + |S| w_{2y}). \quad (43)$$

By comparing to Eq. 33 and Eq. 34 and using the spatial cell size $\delta = \frac{2\pi}{64}$, the value of free modelling constant is retrieved as $c_s = 0.12$.

The SR identified Smagorinsky kernel with $c_s = 0.12$ is plugged into LES source term Π in Eq. 31 and forward LES simulation is run for 2D decaying turbulence problem. Fig. 37 shows the vorticity field at time $t = 4.0$ for DNS, UDNS, FDNS and LES with SR retrieved Smagorinsky kernel. Energy spectrum for the same at time $t = 4.0$ is showed in Fig. 38. We can observe that SR approaches identified the value of modelling constant c_s , that reasonably controls the amount of dissipation needed to account for unresolved small scales.

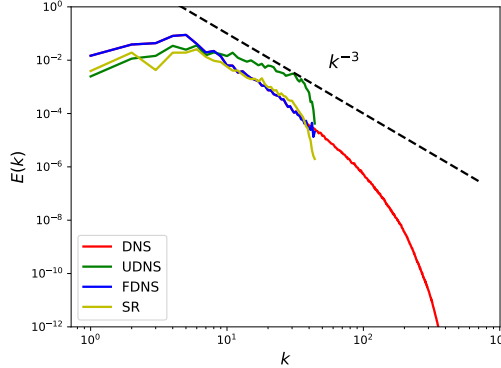


FIG. 38. Energy spectrum for two-dimensional Kraichnan turbulence problem at $t = 4$. SR refers to the identified model of the Smagorinsky kernel with $c_s = 0.12$. UDNS and FDNS refer to the no-model and filtered DNS simulations, respectively.

VI. CONCLUSION

Data driven symbolic regression tools can be extremely useful for researchers to infer complex models from sensor data/measurements when underlying physics is partially or completely unknown. Sparse optimization techniques are envisioned as SR tool that are capable to recover hidden physical laws in a highly efficient computational manner. Popular sparse optimization techniques such as LASSO, ridge and elastic-net are also termed as feature selection methods in machine learning. These techniques are regularized variants of least square regression adapted to reduce overfitting and promote sparsity. Model prediction ability of sparse regression methods is primarily depended on expressive power of its feature library which contains exhaustive combinations of nonlinear basis functions that might represent the unknown physical law. This limits the identification of physical models that are represented by complex functional compositions. GEP which is an evolutionary optimization algorithm is widely adapted for SR approach. This genotype-phenotype algorithm takes advantage of simple chromosome representative of GA and free expansion of complex chromosomes of GP. GEP is a natural feature extractor which may not need apriori information of nonlinear basis other than basic features as terminal set. Generally with enough computational time, GEP may recover unknown physical models that are represented by complex functional compositions by observing the input-response data.

In this paper, we demonstrate sparse regression technique STRidge and evolutionary optimization algorithm GEP in context of effective SR tool in identifying hidden physical laws from observing data. We first identify various canonical PDEs using both STRidge and GEP. We show that STRidge is limited by its feature library for identifying Sine-Gordon PDE. Following equation discovery, we demonstrate the power of both algorithms in identifying the leading truncation error terms for Burgers MDE. While both algorithm find the truncation terms, coefficients found by STRidge were more accurate than coefficients found by GEP. We note that, when feature library is capable of expressing the underlying physical model, application of STRidge is suitable due to its less hyper-parameters and lower computational overhead. Next we illustrate the recovery of hidden physics that is manifested as source or forcing term of a PDE. We use randomly selected sparse measurements that mimic real world data collection. STRidge is not applied to this setting as the feature library was limited to represent the unknown physical model that consists of complex functional compositions. GEP was able to identify the source term for both 1D advection-diffusion PDE and 2D vortex-merger problem using sparse measurements. Finally both STRidge and GEP were applied to discover eddy viscosity kernel along with its ad-hoc modelling coefficient as sub grid scale model for LES equation simulating 2D Kraichnan turbulence problem. This particular example demonstrates the inverse modelling or parametric esti-

mation for turbulence closure models using SR approaches. Future studies are focused on identification of LES closure models that augments the known closure models by accounting for various nonlinear physical process. Furthermore, various SR tools are being investigated for identification of nonlinear truncation error terms of MDEs for implicit LES approaches that can be exploited for modelling the turbulent flows without need for explicit subgrid scale models.

ACKNOWLEDGMENTS

This material is based upon work supported by the U.S. Department of Energy, Office of Science, Office of Advanced Scientific Computing Research under Award Number DE-SC0019290. O.S. gratefully acknowledges their support. Disclaimer: This report was prepared as an account of work sponsored by an agency of the United States Government. Neither the United States Government nor any agency thereof, nor any of their employees, makes any warranty, express or implied, or assumes any legal liability or responsibility for the accuracy, completeness, or usefulness of any information, apparatus, product, or process disclosed, or represents that its use would not infringe privately owned rights. Reference herein to any specific commercial product, process, or service by trade name, trademark, manufacturer, or otherwise does not necessarily constitute or imply its endorsement, recommendation, or favoring by the United States Government or any agency thereof. The views and opinions of authors expressed herein do not necessarily state or reflect those of the United States Government or any agency thereof.

- ¹M. I. Jordan and T. M. Mitchell, "Machine learning: Trends, perspectives, and prospects," *Science* **349**, 255–260 (2015).
- ²V. Marx, "Biology: The big challenges of big data," *Nature* **498**, 255–260 (2013).
- ³F. Rosenblatt, "The perceptron: a probabilistic model for information storage and organization in the brain," *Psychological Review* **65**, 386 (1958).
- ⁴Y. LeCun, Y. Bengio, and G. Hinton, "Deep learning," *Nature* **521**, 436 (2015).
- ⁵E. J. Candes and M. B. Wakin, "An introduction to compressive sampling," *IEEE Signal Processing Magazine* **25**, 21–30 (2008).
- ⁶E. J. Candes and M. B. Wakin, "An introduction to compressive sampling," *IEEE Signal Processing Magazine* **25**, 21–30 (2008).
- ⁷J. R. Koza, *Genetic programming: on the programming of computers by means of natural selection*, Vol. 1 (MIT Press, Cambridge, MA, USA, 1992).
- ⁸C. Ferreira, "Gene expression programming: a new adaptive algorithm for solving problems," *arXiv preprint cs/0102027* (2001).
- ⁹C. Ferreira, *Gene expression programming: mathematical modeling by an artificial intelligence*, Vol. 21 (Springer, 2006).
- ¹⁰M. Mitchell, *An introduction to genetic algorithms* (MIT press, 1998).
- ¹¹J. H. Holland, "Adaptation in natural and artificial systems. 1975," Ann Arbor, MI: University of Michigan Press and (1992).
- ¹²M. Schmidt and H. Lipson, "Distilling free-form natural laws from experimental data," *Science* **324**, 81–85 (2009).
- ¹³J. Bongard and H. Lipson, "Automated reverse engineering of nonlinear dynamical systems," *Proceedings of the National Academy of Sciences* **104**, 9943–9948 (2007).
- ¹⁴Y. Yang, C. Wang, and C. Soh, "Force identification of dynamic systems using genetic programming," *International Journal for Numerical Methods in Engineering* **63**, 1288–1312 (2005).
- ¹⁵L. Ferariu and A. Patelli, "Elite based multiobjective genetic programming for nonlinear system identification," in *International Conference on Adaptive and Natural Computing Algorithms* (Springer, 2009) pp. 233–242.
- ¹⁶C. Luo, Z. Hu, S.-L. Zhang, and Z. Jiang, "Adaptive space transformation: An invariant based method for predicting aerodynamic coefficients of hypersonic vehicles," *Engineering Applications of Artificial Intelligence* **46**, 93–103 (2015).
- ¹⁷S. L. Brunton and B. R. Noack, "Closed-loop turbulence control: progress and challenges," *Applied Mechanics Reviews* **67**, 050801 (2015).
- ¹⁸N. Gautier, J.-L. Aider, T. Duriez, B. Noack, M. Segond, and M. Abel, "Closed-loop separation control using machine learning," *Journal of Fluid Mechanics* **770**, 442–457 (2015).
- ¹⁹T. Duriez, V. Parezanović, K. von Krbek, J.-P. Bonnet, L. Cordier, B. R. Noack, M. Segond, M. Abel, N. Gautier, J.-L. Aider, *et al.*, "Feedback control of turbulent shear flows by genetic programming," *arXiv preprint arXiv:1505.01022* (2015).

²⁰M. Quade, M. Abel, K. Shafi, R. K. Niven, and B. R. Noack, "Prediction of dynamical systems by symbolic regression," *Physical Review E* **94**, 012214 (2016).

²¹C. Luo and S.-L. Zhang, "Parse-matrix evolution for symbolic regression," *Engineering Applications of Artificial Intelligence* **25**, 1182–1193 (2012).

²²M. F. Brameier and W. Banzhaf, *Linear genetic programming* (Springer-Verlag, New York, 2007).

²³R. S. Faradonbeh and M. Monjezi, "Prediction and minimization of blast-induced ground vibration using two robust meta-heuristic algorithms," *Engineering with Computers* **33**, 835–851 (2017).

²⁴R. S. Faradonbeh, A. Salimi, M. Monjezi, A. Ebrahimabadi, and C. Moermann, "Roadheader performance prediction using genetic programming (GP) and gene expression programming (GEP) techniques," *Environmental Earth Sciences* **76**, 584 (2017).

²⁵F. S. Hoseinian, R. S. Faradonbeh, A. Abdollahzadeh, B. Rezai, and S. Soltani-Mohammadi, "Semi-autogenous mill power model development using gene expression programming," *Powder Technology* **308**, 61–69 (2017).

²⁶H. Çanakçı, A. Baykasoglu, and H. Güllü, "Prediction of compressive and tensile strength of Gaziantep basalts via neural networks and gene expression programming," *Neural Computing and Applications* **18**, 1031 (2009).

²⁷J. Weatheritt and R. Sandberg, "A novel evolutionary algorithm applied to algebraic modifications of the rans stress-strain relationship," *Journal of Computational Physics* **325**, 22–37 (2016).

²⁸M. Schoepplein, J. Weatheritt, R. Sandberg, M. Talei, and M. Klein, "Application of an evolutionary algorithm to les modelling of turbulent transport in premixed flames," *Journal of Computational Physics* **374**, 1166–1179 (2018).

²⁹J. Weatheritt and R. D. Sandberg, "Hybrid reynolds-averaged/large-eddy simulation methodology from symbolic regression: formulation and application," *AIAA Journal* , 3734–3746 (2017).

³⁰H. Rauhut, "Compressive sensing and structured random matrices," *Theoretical Foundations and Numerical Methods for Sparse Recovery* **9**, 1–92 (2010).

³¹R. Tibshirani, "Regression shrinkage and selection via the LASSO," *Journal of the Royal Statistical Society: Series B* **58**, 267–288 (1996).

³²G. James, D. Witten, T. Hastie, and R. Tibshirani, *An introduction to statistical learning*, Vol. 112 (Springer Science+Business Media, New York, 2013).

³³R. Tibshirani, M. Wainwright, and T. Hastie, *Statistical learning with sparsity: the LASSO and generalizations* (Chapman and Hall/CRC, Florida, USA, 2015).

³⁴E. J. Candes, J. K. Romberg, and T. Tao, "Stable signal recovery from incomplete and inaccurate measurements," *Communications on Pure and Applied Mathematics: A Journal Issued by the Courant Institute of Mathematical Sciences* **59**, 1207–1223 (2006).

³⁵K. P. Murphy, *Machine learning: a probabilistic perspective* (MIT Press, Cambridge, MA, USA, 2012).

³⁶H. Zou and T. Hastie, "Regularization and variable selection via the elastic net," *Journal of the Royal Statistical Society: Series B (Statistical Methodology)* **67**, 301–320 (2005).

³⁷J. Friedman, T. Hastie, and R. Tibshirani, "Regularization paths for generalized linear models via coordinate descent," *Journal of Statistical Software* **33**, 1 (2010).

³⁸S. L. Brunton, J. L. Proctor, and J. N. Kutz, "Discovering governing equations from data by sparse identification of nonlinear dynamical systems," *Proceedings of the National Academy of Sciences* **113**, 3932–3937 (2016).

³⁹S. H. Rudy, S. L. Brunton, J. L. Proctor, and J. N. Kutz, "Data-driven discovery of partial differential equations," *Science Advances* **3**, e1602614 (2017).

⁴⁰H. Schaeffer, R. Caflisch, C. D. Hauck, and S. Osher, "Sparse dynamics for partial differential equations," *Proceedings of the National Academy of Sciences* **110**, 6634–6639 (2013).

⁴¹H. Schaeffer, "Learning partial differential equations via data discovery and sparse optimization," *Proceedings of the Royal Society A: Mathematical, Physical and Engineering Sciences* **473**, 20160446 (2017).

⁴²G. Tran and R. Ward, "Exact recovery of chaotic systems from highly corrupted data," *Multiscale Modeling & Simulation* **15**, 1108–1129 (2017).

⁴³H. Schaeffer, G. Tran, and R. Ward, "Extracting sparse high-dimensional dynamics from limited data," *SIAM Journal on Applied Mathematics* **78**, 3279–3295 (2018).

⁴⁴N. M. Mangan, J. N. Kutz, S. L. Brunton, and J. L. Proctor, "Model selection for dynamical systems via sparse regression and information criteria," *Proceedings of the Royal Society A: Mathematical, Physical and Engineering Sciences* **473**, 20170009 (2017).

⁴⁵N. M. Mangan, S. L. Brunton, J. L. Proctor, and J. N. Kutz, "Inferring biological networks by sparse identification of nonlinear dynamics," *IEEE Transactions on Molecular, Biological and Multi-Scale Communications* **2**, 52–63 (2016).

⁴⁶J.-C. Loiseau, B. R. Noack, and S. L. Brunton, "Sparse reduced-order modelling: sensor-based dynamics to full-state estimation," *Journal of Fluid Mechanics* **844**, 459–490 (2018).

⁴⁷M. Schmelzer, R. Dwight, and P. Cinnella, "Data-driven deterministic symbolic regression of nonlinear stress-strain relation for rans turbulence modelling," in *2018 Fluid Dynamics Conference* (2018) p. 2900.

⁴⁸P. Zheng, T. Askham, S. L. Brunton, J. N. Kutz, and A. Y. Aravkin, "A unified framework for sparse relaxed regularized regression: SR3," *IEEE Access* **7**, 1404–1423 (2018).

⁴⁹T. Zhang, "Adaptive forward-backward greedy algorithm for sparse learning with linear models," in *Advances in Neural Information Processing Systems* (2009) pp. 1921–1928.

⁵⁰S. Thaler, L. Paehler, and N. A. Adams, "Sparse identification of truncation errors," *Journal of Com-*

putational Physics **397**, 108851 (2019).

⁵¹T. McConaghay, “FFX: Fast, scalable, deterministic symbolic regression technology,” in *Genetic Programming Theory and Practice IX* (Springer, 2011) pp. 235–260.

⁵²H. Vaddireddy and O. San, “Equation discovery using fast function extraction: a deterministic symbolic regression approach,” *Fluids* **4**, 111 (2019).

⁵³M. Schmelzer, R. P. Dwight, and P. Cinnella, “Machine learning of algebraic stress models using deterministic symbolic regression,” arXiv preprint arXiv:1905.07510 (2019).

⁵⁴C. Chen, C. Luo, and Z. Jiang, “Elite bases regression: a real-time algorithm for symbolic regression,” in *2017 13th International Conference on Natural Computation, Fuzzy Systems and Knowledge Discovery (ICNC-FSKD)* (IEEE, 2017) pp. 529–535.

⁵⁵T. Worm and K. Chiu, “Prioritized grammar enumeration: symbolic regression by dynamic programming,” in *Proceedings of the 15th Annual Conference on Genetic and Evolutionary Computation* (ACM, 2013) pp. 1021–1028.

⁵⁶D. Ciregan, U. Meier, and J. Schmidhuber, “Multi-column deep neural networks for image classification,” in *2012 IEEE Conference on Computer Vision and Pattern Recognition* (2012) pp. 3642–3649.

⁵⁷A. Karpathy and L. Fei-Fei, “Deep visual-semantic alignments for generating image descriptions,” in *Proceedings of the IEEE Conference on Computer Vision and Pattern Recognition* (2015) pp. 3128–3137.

⁵⁸A. E. Sallab, M. Abdou, E. Perot, and S. Yogamani, “Deep reinforcement learning framework for autonomous driving,” *Electronic Imaging* **2017**, 70–76 (2017).

⁵⁹M. Raissi, P. Perdikaris, and G. E. Karniadakis, “Physics-informed neural networks: A deep learning framework for solving forward and inverse problems involving nonlinear partial differential equations,” *Journal of Computational Physics* **378**, 686–707 (2019).

⁶⁰M. Raissi, P. Perdikaris, and G. E. Karniadakis, “Numerical gaussian processes for time-dependent and nonlinear partial differential equations,” *SIAM Journal on Scientific Computing* **40**, A172–A198 (2018).

⁶¹J.-F. Cai, B. Dong, S. Osher, and Z. Shen, “Image restoration: total variation, wavelet frames, and beyond,” *Journal of the American Mathematical Society* **25**, 1033–1089 (2012).

⁶²B. Dong, Q. Jiang, and Z. Shen, “Image restoration: Wavelet frame shrinkage, nonlinear evolution PDEs, and beyond,” *Multiscale Modeling & Simulation* **15**, 606–660 (2017).

⁶³Z. Long, Y. Lu, X. Ma, and B. Dong, “PDE-net: Learning PDEs from data,” in *Proceedings of the 35th International Conference on Machine Learning*, Proceedings of Machine Learning Research, Vol. 80, edited by J. Dy and A. Krause (PMLR, Stockholmmsmssan, Stockholm Sweden, 2018) pp. 3208–3216.

⁶⁴Z. Long, Y. Lu, and B. Dong, “PDE-Net 2.0: Learning PDEs from data with a numeric-symbolic hybrid deep network,” *Journal of Computational Physics* **399**, 108925 (2019).

⁶⁵C. Ferreira, “Gene expression programming in problem solving,” in *Soft Computing and Industry* (Springer, 2002) pp. 635–653.

⁶⁶G. Shuhua, “geppy: a gene expression programming framework in python,” <https://github.com/ShuhuaGao/geppy> (2019).

⁶⁷F.-A. Fortin, F.-M. De Rainville, M.-A. Gardner, M. Parizeau, and C. Gagné, “DEAP: Evolutionary algorithms made easy,” *Journal of Machine Learning Research* **13**, 2171–2175 (2012).

⁶⁸R. G. Baraniuk, “Compressive sensing,” *IEEE Signal Processing Magazine* **24** (2007).

⁶⁹H. Bateman, “Some recent researches on the motion of fluids,” *Monthly Weather Review* **43**, 163–170 (1915).

⁷⁰G. B. Whitham, *Linear and nonlinear waves*, Vol. 42 (John Wiley & Sons, 2011).

⁷¹M. Maleewong and S. Sirisup, “On-line and off-line pod assisted projective integral for non-linear problems: A case study with burgers equation,” *International Journal of Mathematical, Computational, Physical, Electrical and Computer Engineering* **5**, 984–992 (2011).

⁷²“On the change of form of long waves advancing in a rectangular canal, and on a new type of long stationary waves,” *Philosophical Magazine* **91**, 1007–1028 (2011), <https://doi.org/10.1080/14786435.2010.547337>.

⁷³L. Wazzan, “A modified tanh-coth method for solving the kdv and the kdv–burgers equations,” *Communications in Nonlinear Science and Numerical Simulation* **14**, 443–450 (2009).

⁷⁴T. Ozis and S. Ozer, “A simple similarity-transformation-iterative scheme applied to Korteweg–de Vries equation,” *Applied Mathematics and Computation* **173**, 19–32 (2006).

⁷⁵G. L. Lamb Jr, *Elements of soliton theory* (Wiley-Interscience, New York, 1980).

⁷⁶T. Kawahara, “Oscillatory solitary waves in dispersive media,” *Journal of the Physical Society of Japan* **33**, 260–264 (1972).

⁷⁷T. Kawahara, N. Sugimoto, and T. Kakutani, “Nonlinear interaction between short and long capillary-gravity waves,” *Journal of the Physical Society of Japan* **39**, 1379–1386 (1975).

⁷⁸J. K. Hunter and J. Scheurle, “Existence of perturbed solitary wave solutions to a model equation for water waves,” *Physica D: Nonlinear Phenomena* **32**, 253–268 (1988).

⁷⁹Sirendaoreji, “New exact travelling wave solutions for the Kawahara and modified Kawahara equations,” *Chaos Solitons & Fractals* **19**, 147–150 (2004).

⁸⁰C. Zhi-Xiong and G. Ben-Yu, “Analytic solutions of the nagumo equation,” *IMA Journal of Applied Mathematics* **48**, 107–115 (1992).

⁸¹J. Nagumo, S. Arimoto, and S. Yoshizawa, “An active pulse transmission line simulating nerve axon,” *Proceedings of the IRE* **50**, 2061–2070 (1962).

⁸²D. G. Aronson and H. F. Weinberger, "Multidimensional nonlinear diffusion arising in population genetics," *Advances in Mathematics* **30**, 33–76 (1978).

⁸³A. Scott, "Neuristor propagation on a tunnel diode loaded transmission line," *Proceedings of the IEEE* **51**, 240–240 (1963).

⁸⁴M. Dehghan and F. Fakhar-Izadi, "Pseudospectral methods for nagumo equation," *International Journal for Numerical Methods in Biomedical Engineering* **27**, 553–561 (2011).

⁸⁵A. Barone, F. Esposito, C. Magee, and A. Scott, "Theory and applications of the sine-gordon equation," *La Rivista del Nuovo Cimento (1971-1977)* **1**, 227–267 (1971).

⁸⁶J. Perring and T. Skyrme, "A model unified field equation," *Nuclear Physics* **31**, 550–555 (1962).

⁸⁷C. W. Hirt, "Heuristic stability theory for finite-difference equations," *Journal of Computational Physics* **2**, 339–355 (1968).

⁸⁸R. D. Richtmyer and K. Norton, *Difference methods for initial value problems* (John Wiley & Sons, New York, 1967).

⁸⁹G. Klopfer and D. McRae, "The nonlinear modified equation approach to analyzing finite difference schemes," in *5th Computational Fluid Dynamics Conference* (1981) p. 1029.

⁹⁰A. Majda and S. Osher, "A systematic approach for correcting nonlinear instabilities," *Numerische Mathematik* **30**, 429–452 (1978).

⁹¹N. Adams, S. Hickel, and S. Franz, "Implicit subgrid-scale modeling by adaptive deconvolution," *Journal of Computational Physics* **200**, 412–431 (2004).

⁹²L. G. Margolin and W. J. Rider, "A rationale for implicit turbulence modelling," *International Journal for Numerical Methods in Fluids* **39**, 821–841 (2002).

⁹³C. Hirsch, *Numerical computation of internal and external flows: The fundamentals of computational fluid dynamics* (Elsevier, Burlington, MA, 2007).

⁹⁴V. M. Krasnopolksy and M. S. Fox-Rabinovitz, "Complex hybrid models combining deterministic and machine learning components for numerical climate modeling and weather prediction," *Neural Networks* **19**, 122–134 (2006).

⁹⁵V. M. Krasnopolksy and M. S. Fox-Rabinovitz, "A new synergetic paradigm in environmental numerical modeling: Hybrid models combining deterministic and machine learning components," *Ecological Modelling* **191**, 5–18 (2006).

⁹⁶S. Dhingra, R. B. Madda, A. H. Gandomi, R. Patan, and M. Daneshmand, "Internet of things mobile-air pollution monitoring system (iot-mobair)," *IEEE Internet of Things Journal* (2019).

⁹⁷N. Kumar, "Unsteady flow against dispersion in finite porous media," *Journal of Hydrology* **63**, 345–358 (1983).

⁹⁸J. Isenberg and C. Gutfinger, "Heat transfer to a draining film," *International Journal of Heat and Mass Transfer* **16**, 505–512 (1973).

⁹⁹V. Guvanasen and R. Volker, "Numerical solutions for solute transport in unconfined aquifers," *International Journal for Numerical Methods in Fluids* **3**, 103–123 (1983).

¹⁰⁰P. Meunier, S. Le Dizès, and T. Leweke, "Physics of vortex merging," *Comptes Rendus Physique* **6**, 431–450 (2005).

¹⁰¹O. San and A. E. Staples, "High-order methods for decaying two-dimensional homogeneous isotropic turbulence," *Computers & Fluids* **63**, 105–127 (2012).

¹⁰²O. San and A. E. Staples, "A coarse-grid projection method for accelerating incompressible flow computations," *Journal of Computational Physics* **233**, 480–508 (2013).

¹⁰³J. N. Reinaud and D. G. Dritschel, "The critical merger distance between two co-rotating quasi-geostrophic vortices," *Journal of Fluid Mechanics* **522**, 357–381 (2005).

¹⁰⁴A. Arakawa, "Computational design for long-term numerical integration of the equations of fluid motion: Two-dimensional incompressible flow. part i," *Journal of Computational Physics* **1**, 119–143 (1966).

¹⁰⁵S. Pawar and O. San, "CFD Julia: A learning module structuring an introductory course on computational fluid dynamics," *Fluids* **4**, 159 (2019).

¹⁰⁶G. Boffetta and S. Musacchio, "Evidence for the double cascade scenario in two-dimensional turbulence," *Physical Review E* **82**, 016307 (2010).

¹⁰⁷G. Boffetta and R. E. Ecke, "Two-dimensional turbulence," *Annual Review of Fluid Mechanics* **44**, 427–451 (2012).

¹⁰⁸R. H. Kraichnan, "Inertial ranges in two-dimensional turbulence," *The Physics of Fluids* **10**, 1417–1423 (1967).

¹⁰⁹G. K. Batchelor, "Computation of the energy spectrum in homogeneous two-dimensional turbulence," *The Physics of Fluids* **12**, II–233 (1969).

¹¹⁰C. Leith, "Atmospheric predictability and two-dimensional turbulence," *Journal of the Atmospheric Sciences* **28**, 145–161 (1971).

¹¹¹U. Piomelli, "Large-eddy simulation: achievements and challenges," *Progress in Aerospace Sciences* **35**, 335–362 (1999).

¹¹²C. Meneveau and J. Katz, "Scale-invariance and turbulence models for large-eddy simulation," *Annual Review of Fluid Mechanics* **32**, 1–32 (2000).

¹¹³P. Sagaut, *Large eddy simulation for incompressible flows: an introduction* (Springer Science & Business Media, 2006).

¹¹⁴J. Smagorinsky, "General circulation experiments with the primitive equations: I. the basic experiment," *Monthly Weather Review* **91**, 99–164 (1963).

¹¹⁵C. E. Leith, "Diffusion approximation for two-dimensional turbulence," *The Physics of Fluids* **11**, 671–672 (1968).

¹¹⁶B. Baldwin and H. Lomax, "Thin-layer approximation and algebraic model for separated turbulent flows," in *16th aerospace sciences meeting* (1978) p. 257.

¹¹⁷A. Smith and T. Cebeci, "Numerical solution of the turbulent-boundary-layer equations," Tech. Rep. (DTIC, 1967).